SYNTHESIS AND CHARACTERIZATION OF NANO-METAL OXIDE ZEOLITES FOR HYDROGEN GAS DETECTION

BY

ANAS AWAD HASAN AHMED

A Thesis Presented to the

DEANSHIP OF GRADUATE STUDIES

KING FAHD UNIVERSITY OF PETROLEUM & MINERALS

DHAHRAN, SAUDI ARABIA

In Partial Fulfillment of the

Requirements for the Degree of

MASTER OF SCIENCE

In

PHYSICS

MAY, 2014

KING FAHD UNIVERSITY OF PETROLEUM & MINERALS

DHAHRAN- 31261, SAUDI ARABIA

DEANSHIP OF GRADUATE STUDIES

This thesis, written by **Anas Awad Hasan Ahmed** under the direction his thesis advisor and approved by his thesis committee, has been presented and accepted by the Dean of Graduate Studies, in partial fulfillment of the requirements for the degree of **MASTER OF SCEINCE IN PHYSICS.**

Dr. Zain Hassan Yamani
(Advisor)

Dr.Abdul-Aziz Al-Jalal
Department Chairman

Dr. Mohamed M. Faiz
(Member)

Prof. Salam A. Zummo
Dean of Graduate Studies

Dr. Muhammad Baseer Haider
(Member)

27/5/14
Date

Dedication

This thesis is dedicated to my deceased father and my mother, wife, son, brothers and sisters.

ACKNOWLEDGMENTS

First and foremost thanks to the Almighty Allah who gave me the strength, ability and patience to accomplish this research work.

I am pleased to express my deep thanks to my Master's thesis advisor, Dr. Zain Yamani, Director of the Center of Excellence in Nanotechnology (CENT) at King Fahd University of Petroleum and Minerals (KFUPM), for his great patience, constant motivation, encouragement and constructive suggestions. I have learned so much from him during this work in so many ways. His skillful scientific guidance during this work enhanced me as a free thinker and an independent researcher.

I also would like to acknowledge and express my deep thanks for my thesis committee members, Dr. M.M. Faiz and Dr. M. Baseer Haider, for their attention and constructive feedback.

I would like to acknowledge the support provided by King Abdulaziz City for Science and Technology (KACST) through the Science & Technology Unit at King Fahd University of Petroleum & Minerals (KFUPM) for funding this work through project No. 09-NAN772-04 as part of the National Science, Technology and Innovation Plan.

I also would like to express my appreciation to Taiz University for the material and scientific support.

I also would like to express my appreciation to CENT, Physics Department, KFUPM, and Imaging Core Lab, KAUST for their assistance during this work.

I am pleased to express my deep thanks to the Chairman of Physics department Dr. A. M. Al-Jalal and my deep thanks to all faculty members of Physics Department, especially who taught and helped me during my study.

I also would like to express my deep thanks to Dr. Ahsanulhaq Qurashi, Dr. Qamar, Dr. Abbas Hakeem, Mr. Ibrar, Mr. Saheed Adewale, Mr. Mohammed Sanhoob, Mr. Idrees and Mr. Muhammad Qamaruddin from CENT for their assistance during the research work. As well, I would like to thank, Mr. Mohammad Said from Physics department for his assistance.

Lastly, I would like to extend my heartfelt thanks to my family, friends for their affection and continued support.

TABLE OF CONTENTS

LIST OF TABLES

LIST OF FIGURES

LIST OF ABBREVIATIONS

SDA	:	Semiconductor device analyzer
LEL	:	Lower explosion limit
UEL	:	Upper explosion limit
IDEs	:	Interdigitated electrodes
MFC	:	Mass flow controller
SCCM	:	Standard cubic centimeter per minute
ppm	:	Parts per million

ABSTRACT

Full Name : [Anas Awad Hasan Ahmed]

Thesis Title : [SYNTHESIS AND CHARACTERIZATION OF NANO-METAL OXIDE ZEOLITES FOR HYDROGEN GAS DETECTION]

Major Field : [PHYSICS]

Date of Degree : [MAY, 2014]

Nano-sized Na-ZSM 5 was synthesized using the hydrothermal method. Sodium ions were exchanged by ammonium hydroxide to get the acidic forms of ZSM 5 and then loaded with metal precursors (zinc acetate, tin acetate, and titanium isopropoxide), and calcined in air at 550℃ for 16 hours to get ZnO loaded ZSM 5, SnO_2 loaded ZSM 5, and TiO_2 load ZSM 5.

The synthesized ZSM 5, ZnO-ZSM 5, SnO_2-ZSM 5, and TiO_2-ZSM 5 were characterized using XRD, FTIR, FESEM, TEM, EDS, and XPS techniques. No peaks corresponding to metal oxides (ZnO, SnO_2, and TiO_2) were observed in XRD spectra. This is probably related to the low loading level of the metal species as well as its high dispersion. FTIR spectra confirmed zeolitic structures. The morphology and size of the synthesized materials were investigated using FESEM and the zeolite crystals were found to be of nanometric dimensions.

The crystalline structure of the synthesized materials was further confirmed using HRTEM. Nano-crystals (approximately 40 nm in size) with well-defined inter spaces were observed. In addition, HRTEM images confirmed the presence of nano-sized metal-

oxide (~5 nm) in ZSM 5. The selected area electron diffraction also confirmed the crystallinity of the synthesized materials.

EDS and XPS analyses confirmed the presence of metal species in the synthesized samples. Furthermore, the oxidation states of elements were investigated using XPS.

The sensing performance of ZnO-ZSM 5, SnO_2-ZSM 5, and TiO_2-ZSM 5 samples to hydrogen gas at different operating temperatures and different concentrations of hydrogen was investigated. The response of hydrogen gas was carried out at 300℃ and 350℃ and at different concentrations of hydrogen (0.05%, 0.1%, 0.2%, 0.4%, 0.6%, 0.8%, and 1%). The response of ZnO-ZSM 5, SnO_2-ZSM 5, and TiO_2-ZSM 5-based sensors at 300℃ and 350℃ was approximately similar. The concentration-dependent response of ZnO-ZSM 5, SnO_2-ZSM 5, and TiO_2-ZSM 5 -based sensors was measured. The results showed that ZnO-ZSM 5-based sensor is more sensitive compared to SnO_2-ZSM 5, and TiO_2-ZSM 5-based sensors. In addition, the response as a function of hydrogen concentration is approximately linear in the range between 0.2% and 1% for all synthesized materials. Furthermore,, the response times of ZnO-ZSM 5, TiO_2-ZSM 5 and SnO_2-ZSM 5 were measured at hydrogen concentration of 1% and they are, approximately, 20s, 34s and 30s, whereas the recovery times are 54s, 64s and 70s, respectively.

ملخص الرسالة

الاسم الكامل:أنس عوض حسن أحمد

عنوان الرسالة: تحضير وفحص الزيولايت نانوية البنية المحملة بأكاسيد المعادن وتطبيقها في الكشف عن غاز الهيدروجين.

التخصص:فيزياء

تاريخ الدرجة العلمية:مايو 2014 م

لقد كان الهدف الأساسي من هذه الدراسة هو تحضير وفحص الزيولايت (نوع ZSM 5) نانوية البنية وتطبيقها في الكشف عن غاز الهيدروجين. حيث تم تحضير (Na-ZSM 5) نانوية البنية باستخدام التسخين المباشر عند درجة حرارة 160 درجة مئوية، لمدة يوم واحد. وللحصول على ZnO-ZSM 5 وSnO_2-ZSM 5 و TiO_2-ZSM 5 ، فقد تم اتباع الخطوات التالية:

أولا: باستخدام طريقة التبادل الأيوني، تم تحويل Na-ZSM 5 الى H-ZSM 5 من خلال استبدال أيونات الصوديوم بهيدروكسيد الأمونيوم . ثانيا: تم تحميلH-ZSM 5 بـ خلات الزنك وخلات القصدير وإيزوبروبوكسيد التيتانيوم، ثم التسخين عند درجة حرارة 550 درجة مئوية، لمدة 16 ساعة من أجل الحصول على ZSM 5 المحملة بأكاسيد المعادن (ZnO-ZSM 5 وSnO_2-ZSM 5 و TiO_2-ZSM 5).

بعد ذلك تم فحص المواد المحضرة باستخدام مجموعة الأجهزة التالية: حيود الأشعة السينية (XRD)، وجهاز التحليل الطيفي بالأشعة تحت الحمراء (FTIR)، والمجهر الإلكتروني الماسح (SEM)، والمجهر الإلكتروني النافذ (TEM)، والتشتت الطيفي للطاقة (EDS) والتحليل الطيفي الفوتوضوئي (XPS).

لقد أثبتت أطياف حيود الأشعة السينية للمواد المحضرة التركيب البلوري لـ ZSM 5، حيث لا يوجد قمم حيود منسوبة لأكاسيد المعادن (SnO_2 و TiO_2 و ZnO)؛ وهذا يمكن تفسيره بأنه نتيجة لنقص تراكيز أكاسيد المعادن، بالإضافة إلى الانتشار الواسع للمعادن في الزيولايت. وقد أكد التحليل الطيفي باستخدام الأشعة تحت الحمراء التركيب البلوري للمواد المحضرة. كما أثبت – أيضا – المجهر الإلكتروني الماسح والمجهر الإلكتروني النافذ الطبيعة النانوية للمواد المحضرة، إضافة

إلى ذلك تم التأكد من التركيب البلوري للمواد المحضرة بواسطة حيود الإلكترونات خلال المواد المحضرة. ولإثبات احتواء ZSM 5 على معادن الزنك والقصدير والتيتانيوم، فقد تم استخدام تقنية التشتت الطيفي للطاقة (EDS) والتحليل الطيفي الفوتوضوئي (XPS) ، وللتأكد أيضا، فقد تم استخدام المجهر الإلكتروني، حيث تم قياس حجم المعادن التى قدرت بـ 5 نانومتر تقريبا.

أخيرا، اختبرت هذه الدراسة كلا من ZnO-ZSM 5 وSnO_2-ZSM 5 و TiO_2-ZSM 5 ؛ لاستكشاف غاز الهيدروجين عند تراكيز مختلفة للهيدروجين (0.05% و 0.1% و 0.2% و 0.4% و 0.6% و 0.8% و 1%)، وعند درجات حرارة مختلفة (300 و 350 درجة مئوية)، حيث وجد أن الاستجابة للمواد المحضرة متساوية تقريبا عند 300 و 350 درجة مئوية. وقد لاحظنا في هذه الدراسة استجابة كل من ZnO-ZSM 5 وSnO_2-ZSM 5 و TiO_2-ZSM 5 للتراكيز المختلفة لغاز الهيدروجين؛ فكانت تقريبا خطية على مدى ما بين 0.2% و 1% . إلى جانب ذلك تبين أن ZnO-ZSM 5 تملك أعلى استجابة لغاز الهيدروجين مقارنة بـ SnO_2-ZSM 5 و TiO_2-ZSM

CHAPTER 1

INTRODUCTION

The atmospheric air around us contains different kinds of gases, some of which have natural origins and are vital to human life, whereas many others have artificial origins and are dangerous to human life if exceeded certain levels [1, 2]. Industrial processes increasingly involve using dangerous emissions of gases that pollute the environment and cause risks to the public health. Therefore, gas sensors are needed to measure the pollution level in the atmosphere so that appropriate steps can be followed to control the pollution. In addition, there is a need for gas sensors to monitor flammable and toxic gases in order to protect humans from undesirable incidents such as asphyxiation, fire, and death to people working in industrial plants and living nearby [3]. Gas sensors play an important role in both industrial processes and domestic houses, where monitoring and controlling of gases are needed. For instance, they are used for detecting harmful gases in chemical and petrochemical industries, aerospace agencies, food and drink production companies, scientific and engineering research institutes, and in medical and healthcare sectors [3, 4].

The history of semiconducting metal oxide gas sensors is linked to the discovery of Brattain and Bardeen, more than 50 years ago. They discovered that electrical properties of a semiconductor change due to gas adsorption [5]. Since then, detailed studies on semiconductor metal oxides were carried out with a variety of gaseous

species. For example, the chemiresistive semiconductor metal oxide gas sensor was reported for the first time in 1962, by Seiyama and his co-workers, when they noticed that the conductivity of ZnO thin films, heated to 300℃, changed due to reactive gases present in the air [6]. Not long after, the same behaviour for SnO_2 was reported by Taguchi, who issued a patent for the invention of the first commercial gas sensor based on SnO_2[7]. From that time onward, semiconducting metal oxides (like: ZnO, SnO_2, WO_3, In_2O_3) and mixed oxides (like: $LaFeO_3$, $BaTiO_3$, $ZnFe_2O_3$, $SnO_2 - In_2O_3$) [3, 4] have been studied extensively[1, 2, 8-13] for gas sensing properties and applications.

1.1. The Importance of Hydrogen Detection

Recent studies suggest hydrogen as the next clean fuel candidate [14] for many reasons:

- The product of its burning is purely water vapour.
- Hydrogen can be produced from water through electrolysis, or from hydrocarbons by steam reforming
- It has gravimetric efficiency. "The amount of energy produced by hydrogen, per unit weight of fuel, is about three times the energy contained in an equal weight of gasoline and nearly seven times that of coal" [15].

The above-mentioned advantages make hydrogen suitable for various applications. For example, NASA has been using hydrogen fuel cells to provide the electricity of space

shuttles [14]. Hydrogen is also a feed for some petrochemical processes, and is used in oil desulfurization [16].

In recent years, researchers have focused on how to make hydrogen as a cost effective fuel, so that it may be considered as future societies' fuel. On the other hand, hydrogen is highly flammable gas. Hydrogen is considered as a reducing agent, and has ability to pass through many materials; hence, it needs special caution in storage and handling [16].

Hydrogen is colourless, odourless, tasteless, and flammable gas; it is not detectable by human senses. This implies that devices must be used to detect its presence. In terms of its safety, monitoring and controlling of its concentration is necessary in various industrial areas, such as the production of rocket fuels, hydration of hydrocarbons, and methanol and ammonia synthesis. Furthermore, in metallurgical processes, it is important to measure hydrogen concentration. For instance, during aluminum melting, the metal can react with water to produce alumina and hydrogen [17].

In addition, measurement of hydrogen concentration is important in nuclear power plants, where hydrogen can be produced, during plutonium reprocessing, by radiolysis of water, or by undesirable reaction of water with cladding materials such as uranium oxide or zirconium, at high temperature inside reactor cores [17]. In previous decades, dangerous accidents related to hydrogen have occurred. For example, in 1989, hydrogen explosion in a polyethylene plant, at Pasadena, Houston (USA), killed 22 and wounded 100 people [17]. Furthermore, hydrogen explosion contributed to the nuclear accidents at Fukushima Daiichi and Three Mile Island nuclear power plants [18].

Table 1 illustrates the lower explosion limit (LEL) and the upper explosion limit (UEL) of gasoline, propane, ethane, hydrogen, methane, and propylene. Among the listed fuels, hydrogen has the widest range (4-75% by volume in air) of flammability, so that it is important to have hydrogen gas sensors with a wide measurement range. Since hydrogen is the lightest and smallest molecule, it is likely to diffuse through materials and leaks occur. Therefore, hydrogen leak detection is considered as a high priority during production, transportation, and storage.

Table 1-1 Explosive limits for common constituents in process industries [16].

Fuel	Lower Explosion Limit (%)	Upper Explosion Limit(%)
Gasoline	1.4	7.6
Propane	2.1	10.1
Ethan	3	12.4
Hydrogen	4	75
Methane	5	15
Propylene	2.0	11.1

1.2. Gas Sensors Classifications

Chemical gas sensors can be defined as devices that convert the concentration of a target gas into an electronic signal. Various methods can be used for gas sensors classification [3, 18, 19]. For instance, taking into account the change in the electrical and optical properties of sensing materials in the presence of target gases, gas sensors can be classified into three groups: (1) mass-sensitive gas sensors, (2) optical gas sensors, and (3) chemiresistive gas sensors.

1.2.1. Mass-sensitive Gas Sensors

Mass-sensitive or piezoelectric based gas sensors such as, quartz crystal microbalance (QCM), microcantilever, and surface acoustic wave (SAW)-based sensors depend on a mass change due to the accumulation of the analyzing gas when it interacts with the sensing layer, where the mass change can be expressed as a function of a frequency shift [18]. Figure 1-1 shows a typical structure of a surface acoustic wave sensor. It consists of a piezoelectric substrate, two inter-digitated transducers (IDTs), and a sensing layer.

The operation principle is basically based on the inverse piezoelectric effect. Applying an oscillating electric field on piezoelectric materials creates a mechanical wave which in turn propagates along the surface and then converted back to an electrical signal for measurements. The interaction of the analyzing gases with the sensing material deposited on the substrate causes a mass change of the sensing layer which is proportional to a frequency shift of the measured electrical signal.

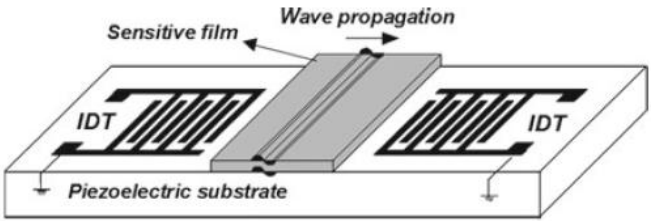

Figure 1-1 Schematic of a surface acoustic wave (SAW) gas sensor [3].

1.2.2. Chemiresistive Gas Sensor

This kind of sensor usually has a simple structure, and its detection principle is based on measuring a change in electrical conductivity of a sensing material when it interacts with a target gas. Figure 1-2 shows a typical structure of such a chemiresistive gas sensor. It consists of three basic elements: an insulating substrate, interdigitated transducers (IDTs), and a sensitive layer. The sensing performance is enhanced by heating the sensing material, often using a heater under the substrate, to a certain temperature, which called the "operating temperature".

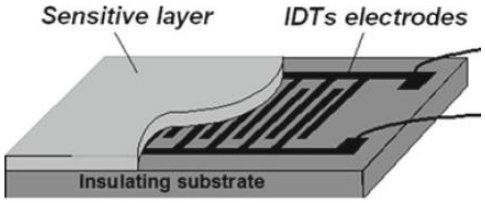

Figure 1-2 Schematic of a chemiresistive gas sensor [3].

Semiconductor materials are commonly used as sensing materials for reducing gases such as H_2, CO, and hydrocarbons. The detailed sensing mechanism of semiconductor gas

sensors is complicated. Yet, it is commonly accepted that the mechanism is considered as a surface effect in which the conductivity of the sensing material is changed due to adsorption and chemical reactions taking place on the surface of the sensing material. Two main reactions are involved in the chemiresistive sensor-mechanism. First, atmospheric oxygen is adsorbed on the surface of n-type semiconductor materials such as SnO_2 or ZnO in the forms of $O_2^-, O^- and O^{2-}$ (depending on operating temperatures) which results in consuming of electrons [3, 18]:

$$O_{2(gas)} + 2e^- \leftrightarrow 2O^-_{(ads)}$$

The trapping of electrons from the surface causes decreasing in the conductivity of n-type semiconductor which form a depletion region. Second, introducing reducing gases, for example H_2 desorbs the adsorbed oxygen according to the following equation:

$$H_{2(gas)} + O^-_{(ads)} \rightarrow H_2O + e^-$$

resulting in releasing the trapped electrons to the conduction band, thus increasing the conductivity of the semiconductor. The concentrations of oxidizing or reducing gases can be measured by monitoring the changes in the conductivity of the semiconducting material.

1.2.3. Optical Gas Sensors

Generally, optical gas sensors are based on the interaction of electromagnetic waves (i.e. IR or UV) with chemicals. The basic elements of optical gas devices are: (1) a light source, (2) monochromator, (3) a sensing element, (4) a transducer for converting the changes in optical properties into measurable signals.

The detection principle of optical gas sensors can be classified into two types. In first type, ananalyte can be used as a sensing material, where its intrinsic optical property is used for its detection. In the second type, an indicator sensing is utilized in case the analyte has no intrinsic optical property and it mainly utilizes ultraviolet and infrared spectroscopes.

Optical absorption, chemiluminescence, and fluorescence techniques are widely employed in optical gas devices [49-51]. For instance, the concentration of the analyte, which has an intrinsic optical property, can be examined directly by measuring characteristic absorption properties of the gas molecule (the analyte) in the infrared range of the electromagnetic spectrum. Gas species can be detected either by measuring the optical absorption at IR wavelengths such as, CH_4, CO, CO_2, NH_3 or by measuring the optical absorption at UV wavelengths such as ,O_3, H_2S, NO_2. On the other hand, indicator dyes are utilized as extrinsic sensors to detect the target gas in case the latter has no intrinsic optical property. The operating principle here is based on the variation of the optical properties (i.e., absorption, fluorescence) of the indicator dyes when interacted with target molecules.

1.3. Characteristics of Gas Sensors

The electrical resistance of a chemiresistive gas sensor increase or decrease considerably when exposed to target gas molecules. Table 1 shows the nature of sensing material (n-type or p-type) for target (reducing or oxidizing) gases.

Table 1-2 The resistance behavior of semiconducting materials

Sensing material	Reducing gases	Oxidizing gases
n-type	Resistance decrease	Resistance increase
p-type	Resistance increase	Resistance decrease

The response of a chemiresistive gas sensor is characterized by the following parameters:

1.3.1. Sensitivity

Many approaches can be used to define the sensitivity (S) of a gas sensor. The common definitions are**:**

A ratio of the resistance in air to the resistance after exposure to an analyte gas [4]

$$S = \frac{R_{air}}{R_{gas}} \qquad \text{for n-type sensing materials}$$

$$S = \frac{R_{air}}{R_{gas}} \qquad \text{for p-type sensing materials}$$

A high value of S means the sensing material is a very good sensor. In addition, a percentage definition of the response can be used:

$\text{Response}(\%) = \left(\frac{R_{air} - R_{gas}}{R_{air}}\right) \times 100.$ A positive value of the response means that the resistance of a sensing material decrease when exposed to an analyte gas and vice versa [4].

1.3.2. Selectivity

Most chemiresistive gas sensors exhibit high sensitivity toward many gases under the same operating conditions. This is generally an undesirable property as the type of gas is then not speculated. Gas sensors, which can select the gas intended and ignore the interfering gases, are the preferred ones. Thus, the selectivity of a sensor can be expressed by:

$$\text{Selectivity} = \frac{\text{Sensitivity towards the desired gas}}{\text{Sensitivity of the sensor for interfering gas}}$$

1.3.3. Response time

The response time is defined as the time interval required to reach a fixed percentage (usually 90%) of the final change in the conductance when the sensor is exposed to the gas [4]. A good and an applicable sensor should have small response time.

1.3.4. Recovery time

The recovery time is defined as the time required for the conductance to drop back to 10% of the saturation value when the sensor is exposed to clean air. Small recovery times are preferred.

1.3.5. Long-term Stability

Stability is an important aspect for evaluating the performance of gas sensors. It is defined as the ability of the sensor to keep its sensing properties without changing when it operates continuously for long periods in harsh environment [4]. Good sensors are expected to work for long durations, several years, without exhibiting drifts in their sensitivity, selectivity, and response-recovery times.

CHAPTER 2

LITERATURE REVIEW

2.1. Zeolite-Based Gas Sensors

Zeolites are inorganic, crystalline aluminoslicate materials which have pores and channels of molecular sizes. Zeolitic structures are composed of interconnected aluminosilicate building units, i.e., SiO_4or AlO_4tetrahedra, linked by sharing oxygen atoms to form three-dimensional frameworks. Figure 2-1 shows the grouping of SiO_4 tetrahedron to form 3D framework. The pure silicalite framework is electrically neutral, but by replacing Si^{+4} with Al^{+3} ion,the total aluminosilicate framework becomes negatively charged which must be compensated by extra-framework cations, such as Na^+, K^+, etc. The empirical formula of zeolites is:

$$M_{y/m}^{+m}\left[(\mathrm{Si}O_2)_x.(\mathrm{Al}O_2{}^-)_y\right].nH_2O$$

where M is an extra-framework cation with charge m. x/y is the silicon to aluminum ratio of the framework. As illustrated the formula above, inserting Al^{3+} into zeolite's framework creates a negative charge which must be compensated by y/m cations M^{m+}. According to Lowenstein rule [20],$\frac{Si}{Al} \geq 1$, meaning that Al-O-Si and Si-O-Si bonds are allowed, whereas Al-O-Al bonds are forbidden due to the repulsive forces between adjacent $\mathrm{Al}O_4{}^-$[20-23].

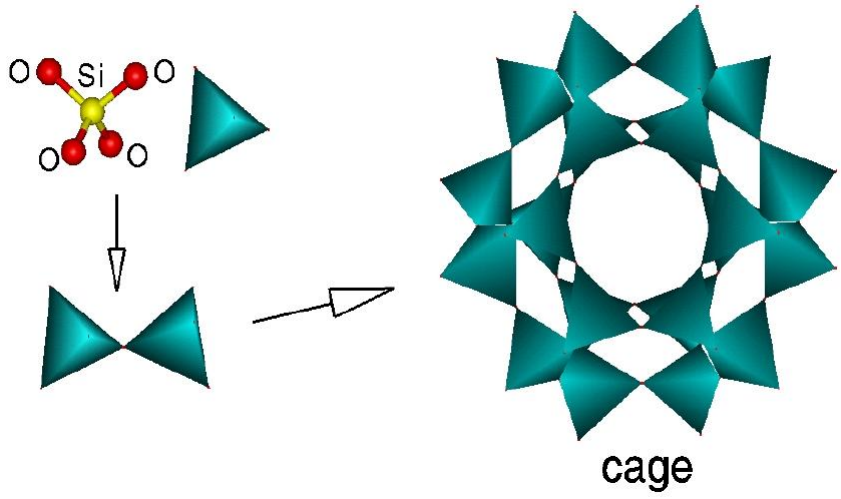

Figure 2-1 The gathering of SiO_4 tetrahedron to form zeolite framework [24].

Zeolite properties, including: adsorption, ion-exchange capacity, molecular sieving, catalysis, and conductivity can be effectively adjusted by changing $\frac{Si}{Al}$ratio. For example, zeolites are hydrophilic if the silicon to aluminum ratio is low, which can be exploited as drying agents; on the other hand, in case of a high silicon to aluminum ratio, the zeolites are hydrophobic, and can be used for extracting organic compounds from water or moist air [25].

The properties mentioned above of zeolites have been used in enhancing gas sensors. Zeolite-based gas sensors can be classified into two types [26]. On the one hand, zeolites may act as sensing medium. In this type, the detection principle of sensors depends directly on the interaction of adsorptive, conductive or catalytic properties of zeolite and their ambient atmosphere. The second type includes sensors in which zeolites act as auxiliary elements. For instance, the sensing material (i.e., SnO_2) is coated by a layer of zeolite or the sensing material can be encapsulated within cages and channels of zeolites.

2.2. Adsorption of Molecules in Zeolites

The adsorption property of zeolites has been employed in gas sensor devices.

Figure 2-2 shows conceptually the change in a mass of zeolite Y due to adsorption of acetone molecule into its supercage.

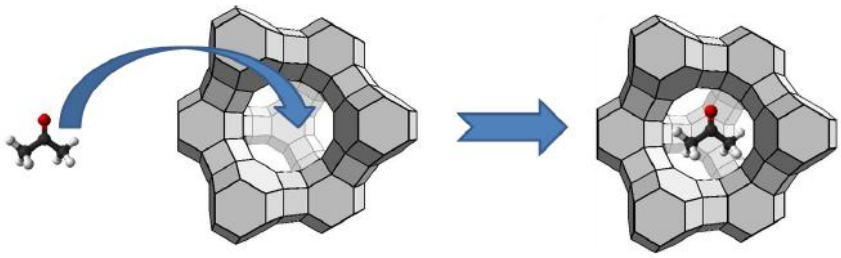

Figure 2-2 Acetone adsorption into zeolite Y supercage [27].

Due to the adsorption property of zeolite's framework, a wide range of gas sensor studies investigate the application of zeolite layers onto mass-sensitive sensors, like quartz crystal microbalances (QCM), microcantilevers, and surface acoustic waves (SAW) sensors, as a sensing medium [28-34]. In this type of sensors, the adsorption of gas molecules onto the sensing medium result in a mass change which in turn is proportional to a frequency shift of the sensor. A number of publications studying the adsorption of an analyte gas within zeolite frameworks are available in the literature. Mintova and Bein, for instance, investigated LTA and BEA zeolites coated on QCM to detect the humidity in water [28, 29]. Zhou et al. reported that ZSM-5 deposited on a microcantilever is used

to detect Freon-12, and showed high selectivity (no interference to ethanol) [30], while Huang et al. studied Ag-ZSM-5 layer deposited on QCM as acetone sensors for diabetes diagnosis [31]. In ref. [32], silicalite-1 film coated SAW devices for detecting moisture, acetone, and benzene.

In addition, an alternative approach is using the adsorption of analytes in zeolites to design optical devices. Here, the refractive index is changed due to adsorption of organic vapors. For this purpose, pure silica (i.e. silicalite) thin film is deposited on an optical fiber [33] or coated onto Attenuated Total Reflectance (ATR) crystals [34].

2.3. Diffusion Discrimination of Analytes through Zeolites

As known, the conventional p- or n-type semiconducting gas sensors have a lack of selectivity. Zeolites as filters can be exploited for improving the selectivity of these conventional sensors. For example, covering a sensing material by a zeolite layer causes blockage of interfering gases, thereby preventing their interaction with the sensing material. This approach of selectivity improvement has been investigated in the literature for a wide variety of semiconducting-zeolite gas sensors, e.g., silicalite and zeolite-A deposited on Pd-doped SnO_2 [35, 36], acidic zeolites (H-A, H-Y, H-ZSM-5) coated on chromium titanium oxide (CTO) and WO_3 [37], silicalite-1 on SnO_2 thin films [38], Ferrierite zeolites on$La_2O_3 - Au/SnO_2$[39], Mordenite zeolite on SnO_2[40], Cr-loaded zeolite-Y on $Cr_{2-x}Ti_xO_y$[41, 42]. The effect of the zeolite layer on the sensor performance is illustrated in Figure 2-3. As illustrated, the uncoated sensor shows a pronounced cross-interference, whereas the selectivity of the zeolite coated sensor was

markedly improved. An extensive discussion of this type of application can be found in Ref. [43]. Filter properties can be controlled by modifying the zeolite type [35], its mobile ions [44], and metal loading [45].

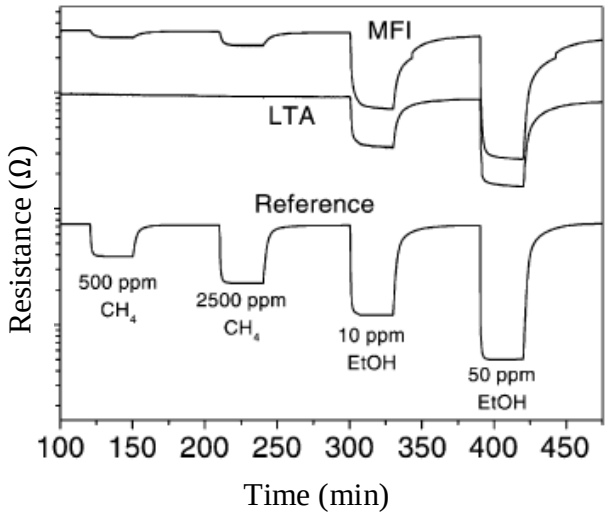

Figure 2-3 Selectivity improvement of pd-doped SnO_2 sensor using zeolite film [35].

2.4. Zeolites as Hosts

The intra-zeolitic spaces of zeolites have been exploited in gas detection sensors. They serve as host for guest species that react in specific manners with an analyte of interest. Since zeolite FAU has large pores (supercages) [23], it is convenient to encapsulate some dye molecules or complexes. The ruthenium (II) bipyridyl complex ($Ru^{+2}(bpy)_3$), an excellent fluorescent oxygen probe, was encapsulated in FAU zeolite via ion-exchange reaction using ruthenium (III) chloride as a starting material. To build a sensor, the sensing materials are incorporated into silicone polymers and spread, in form of a thin layer, on a polyester support. The obtained sensing materials are examined with respect to the quenching of luminescence intensity by molecular oxygen, leading to detectable responses. Oxygen was measured over the 0-760 Torr range. A very good resolution was observed in the range (0-200 Torr) [34]. In addition, $[Ru(bpy)_3]^{+2}$ was prepared inside the supercages of highly siliceous FAU zeolites for dissolved oxygen detection [47, 48].

Zou et al. incorporated LiCl into Stilbte zeolite, and a high sensitive humidity performance over the whole range of relative humidity was achieved with a linear change of 4 orders in magnitude of electrical conductivity. Furthermore, fast responses and favorable reversibility were obtained to environmental humidity changes [49]. Similarly, loading LiCl into Na-Y zeolite was reported in Ref [50], where some problems of the bulk LiCl salt, such as durability and stability at high temperature and high humidity were solved using guest/host material of LiCl/Na- zeolite Y.

Other examples of zeolite guest/host sensors, which are optical in nature, were also investigated. The variations of spectroscopic properties of dye molecules incorporated into zeolite cavities due to the interaction with analytes were exploited in gas detection sensors. For example, protonation or deprotonation of methylene bluein H-mordenite zeolite varies as a function of humidity level. This was probed using diffuse reflectance spectroscopy, and the sensor showed a linear response in relative humidity in the range 9-92%. The sensor operates at either 560 nm absorption band or 745 nm absorption band but a higher sensitivity was observed at the 650 nm band [51, 52]. Pellejero, et al. developed an optical reflectance sensor based on the solvatochromic Nile red dye in Na-Y zeolite supercages. The sensor showed detection limits lower than 200 ppm and response time around 4 min. The differentiation against hexane was attributed to the weak adsorption on hydrophilic zeolite Y [53].

CHAPTER 3

Synthesis and Characterization Techniques

3.1. Synthesis of ZSM 5

ZSM-5was synthesized using the hydrothermal method. Aluminum isopropoxide and tetrapropylammonium hydroxide (TPAOH) solutions were mixed. Small amounts of NaOH were dissolved in H_2O and added to the previous solution and then stirred for making the mixture homogenously distributed. Next step is adding tetraethyl orthosilicate (TEOS) to the clear solution. In order to get a complete hydrolysis of the aluminum and silicon sources, the mixture was stirred for 24 hrs. The composition of the final clear solution is: 9TPAOH: 0.16NaOH: Al: 25Si: $300H_2O$. In order to remove the excess sodium, thorough washing was carried out by water. The final clear solution was transferred into an autoclave vessel (as shown in Figure 3-1) and heated at 160℃ for 24 hours in order to get a colloidal solution. Afterwards, the colloidal solution was centrifuged followed by drying and calcination at 450℃ for 16 hours in order to get the final Na-ZSM-5 powder [54-56].

Figure 3-1 Photograph of autoclave vessel (left) and the inner Teflon container (right).

3.1.1. Ion-exchange of ZSM 5

The next step is the ion exchange reaction, in which sodium ions in the zeolite framework were ion exchanged for protons to get acidic form of zeolite (H-ZSM-5). The sodium product was placed in a conical flask and then stirred with an aqueous ammonium hydroxide for 24 hours at room temperature. Next, the solution was centrifuged and washed several times with de-ionized water to collect H-ZSM-5 and then dried.

3.1.2. Metal Oxides Loading of ZSM 5

The final step is to form nano-metal oxide zeolites. To get ZnO-ZSM-5, SnO_2-ZSM-5, and TiO_2-ZSM-5, 20% by weight of zinc acetate, tin acetate, and titanium tetra-isopropoxide were added to H-ZSM-5 and ethanol in flask. The solution was stirred for 24 hours at room temperature (see Figure 3-2a). The mixture was then centrifuged, washed, and dried. Finally, the products (Zn-ZSM-5, Sn-ZSM-5, and Ti-ZSM-5) were calcined at 550℃ for 16 hours to get ZnO-ZSM-5, SnO_2-ZSM-5, and TiO_2-ZSM-5. The resulting materials (depicted in Figure 3-2b) were sent for characterization to confirm the synthesis of nano-metal oxide zeolites.

(a) **(b)**

Figure 3-2: (a) Photograph of the reaction of loading ZSM 5 with Ti, (b) Photograph of TiO_2-ZSM 5

3.2. Characterization Techniques

3.2.1. XRD Measurements

X-ray diffraction spectra were carried out by a Rigaku diffractometer (MiniFlex II), as shown in Figure 3-3a, located at the Center of Excellence in Nanotechnology (CENT), King Fahd University of Petroleum and Minerals (KFUPM). It was operated at voltage of 30 kV and a current of 15 mA, with $Cu\ K_\alpha$ radiation. XRD spectra were performed in the range of $5^\circ - 70^\circ$ with scan speed of 2 deg./min. and step width of 0.02 deg.

X-rays diffraction is a powerful technique used to identify unknown materials and to study their crystalline structure. High energy electrons (emitted from a filament and accelerated under high voltage) bombard the inner shells of target atoms (Copper) to produce the characteristic X-rays. The produced characteristic x-rays pass through monochromator to select a monochromatic radiation (Cu $K_\alpha, \lambda = 0.1540\ nm$).The monochromatic radiation is directed to the sample and reflected and then detected (see Figure 3-3b).

XRD is based on the constructive interference of monochromatic X-rays (Cu $K_\alpha, \lambda = 0.1540\ nm$) by a crystalline sample. The constructive diffraction occurs when Bragg's law is satisfied (see Figure 3-3c):

$$n\lambda = 2d\sin\theta$$

where, n is an integer, λ is the wavelength of the incident beam, d is the distance between atomic planes, and θ is the ingle between the incident beam and a scattering plane.

.

(a)

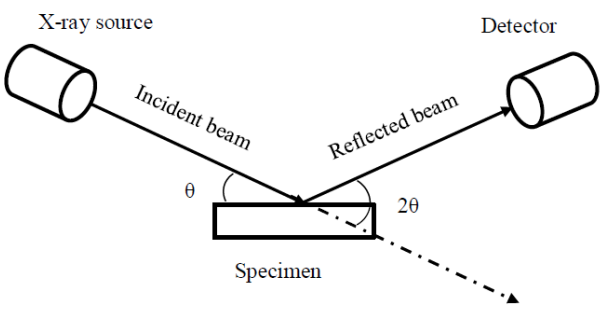

(b)

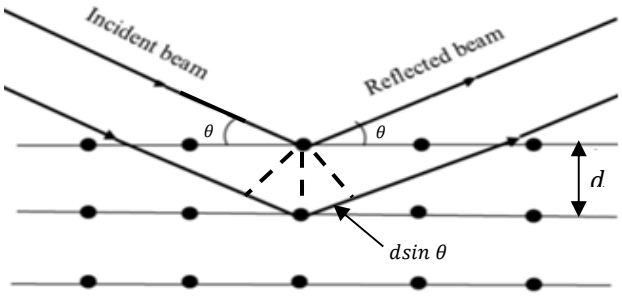

(c)

Figure 3-3: (a) Photograph of the MiniFlex II Rigaku difrractometer unit, (b) Basic components of XRD unit, (c) Schematic diagram of Bragg diffraction.

3.2.2. X-ray Photoelectron Spectroscopy (XPS)

XPS spectra were carried out using Escalab 250 Xi (thermo scientific), located at the Surface Science Laboratory, Physics Department, King Fahd University of Petroleum and Minerals (KFUPM). A photograph of the system is depicted in Fig. 3-4a.

XPS technique provides information about the compositions present at the surface of the sample. Figure 3-4b shows the schematic diagram of XPS. A sample is placed in ultra-high vacuum (UHV) chamber (~10^{-10} mbar) for avoiding contamination and losing electrons due to scattering with gas molecules. A monoenergetic Al K_α (1486.6 eV) X-ray photons strike the surface of the sample resulting in ejection of inner shell electrons of the sample (as seen in Figure 3-4c). The ejected electrons transport through focusing optics to energy analyzer, which distinguishes between the electrons depending on their kinetic energies, and then detected by the detector. According to the photoelectric effect, the energy of the incident photon on a sample is related to the kinetic energy of the ejected electron and the binding energy of the electron by:

$$\mathrm{E_b} = \mathrm{h\nu} - \mathrm{E_K} - \mathrm{W}$$

where $E_b$and E_K are respectively the binding and the kinetic energy of the ejected electron, $h\nu$ is the photon energy, and W is the spectrometer work function [57]. The quantities on the right-hand side are known or measurable, so the binding energy of the ejected electron can be calculated.

(a)

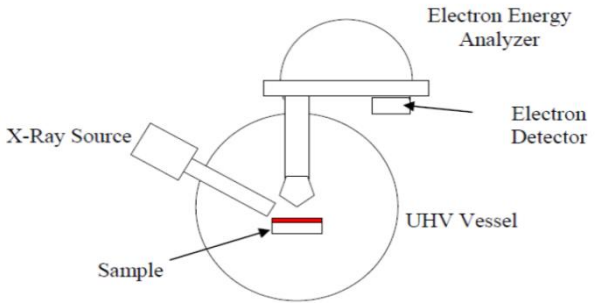

(b)

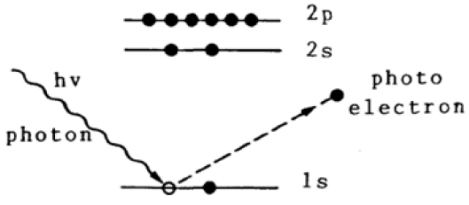

(c)

Figure 3-4: (a) Photograph of XPS, (b) Schematic diagram of XPS, (c) The basic principle of XPS.

3.2.3. Field Emission Scanning Electron Microscopy (FESEM)

The morphology of nano-metal oxide zeolites was carried out using Field Emission Scanning Electron Microscopy (TESCAN), as seen in Figure 3-5a, located at Center of Excellence in Nanotechnology (CENT), King Fahd University of Petroleum and Minerals (KFUPM). It is also equipped with an X-ray energy dispersive spectroscope (EDS) detector (OXFORD X-Max) for quantitative analysis.

In this technique, a sample is placed in high vacuum environment and irradiated by focused electron beam. Due to the interaction between the incident electron beam and the sample, secondary electrons (SE), backscattered electrons (BSE), characteristic x-rays and other signals are generated as shown in Figure 3-5b. However, secondary electrons are generated near the surface of the sample due to the inelastic collisions of incident electrons with the surface. SEs emitted from the surface are collected and processed to get images which reflect the fine microstructure of the sample. In addition, the elemental composition of the sample at the surface can be calculated by detecting the characteristic X-rays emitted from the surface of the sample [58].

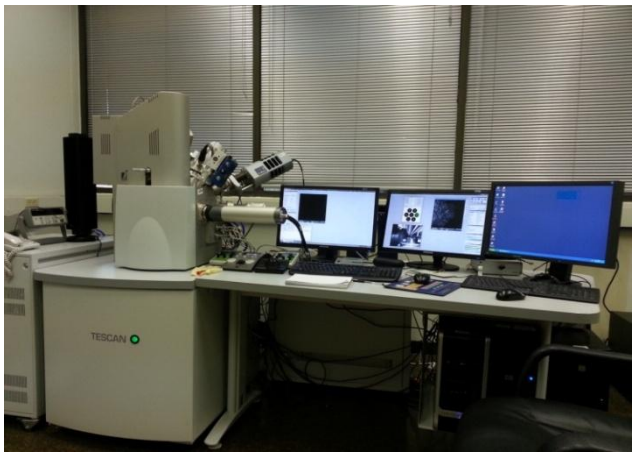

(a)

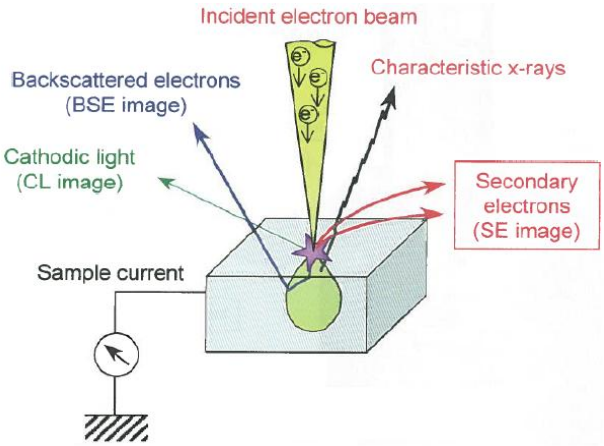

(b)

Figure 3-5: (a) Photograph of FESEM unit captured from imaging lab, CENT, (b) The principle of SEM.

3.2.4. High Resolution Transmission Electron Microscopy (HRTEM)

The confirmation of nanostructured nature and crystalline structure of synthesized materials was carried out using high resolution transmission electron microscopy (FEI, Titan 80-300 CT), as seen in Fig. 3-6, located at imaging and characterization core lab, King Abdullah University of Science and Technology (KAUST).

Transmission electron microscopy is a powerful technique for structure analysis. An electron beam from a source penetrates the material under study, creating patterns and images of the materials on fluorescent or digital screen. TEM can be used to identify the crystalline structure of the materials (through images and selected area electron diffraction (SAED)), determine unknown materials (using EDS), and study structural

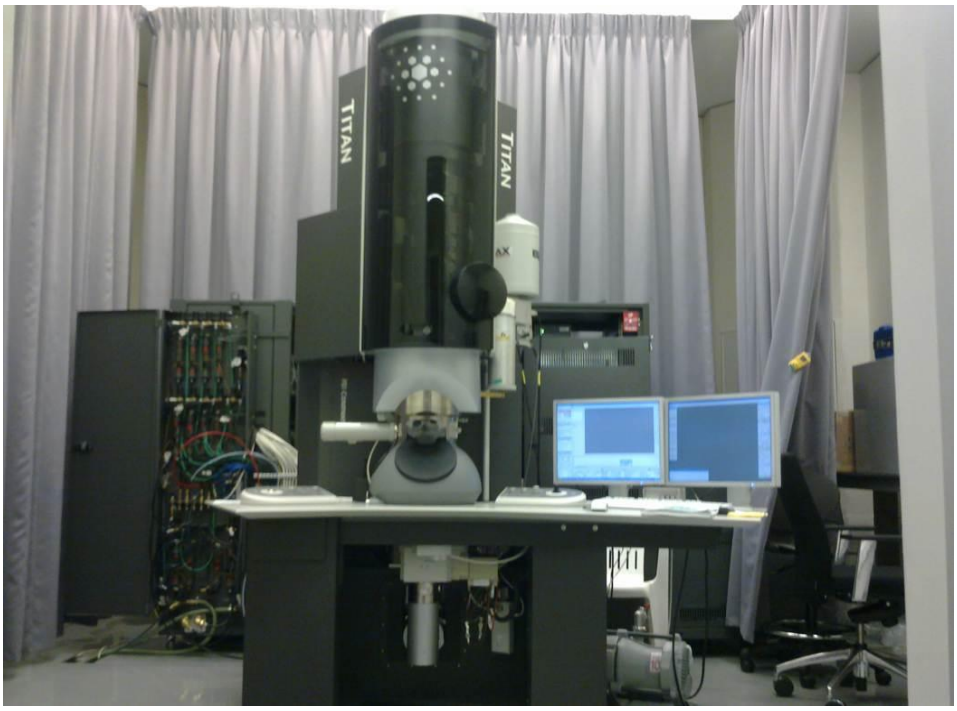

Figure 3-6 Photograph of HRTEM unit taken from imaging and characterization core lab, KAUST

3.2.5. Fourier Transform Infrared Spectroscopy (FTIR)

Transmission FT-IR spectra were recorded using a Nicolet 6700 (thermo scientific) FT-IR spectrophotometer (as seen in Figure 3-7a), located in Center of Excellence in Nanotechnology (CENT), King Fahd University of Petroleum and Minerals (KFUPM).All FT-IR spectra were measured in the range of $400 - 4000\ cm^{-1}$ using KBr as a standard reference.

FTIR spectroscopy is used to identify unknown materials. Since each material has a unique configuration of atoms, the IR spectroscopy can be used to get information about the absorption peaks corresponding to the vibrations between the bonds of the atoms consisting of the material. Figure 3-7b shows the basic components of FTIR spectrophotometer. As shown, the light from a source is directed to the beam splitter, which split the beam into two beams. One beam is directed to stationery mirror and the other beam is directed to a movable mirror. The beams reflected from the mirrors are recombined at the beam splitter. Interference occurs due to the path difference between the recombined beams. The resulting signal from the interferometer is measured as a function of the path difference of the two beams and called the interferogram. IR spectrum is recorded by executing the Fourier transform of the interferogram [59].

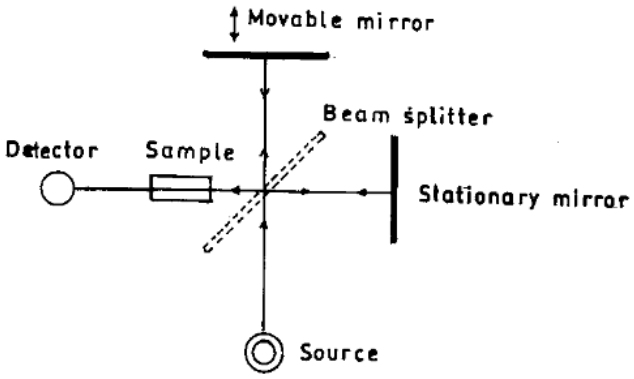

(a) **(b)**

Figure 3-7: (a) Photograph of FTIR spectrophotometer unit taken from CENT lab, (b) Schematic diagram of FTIR spectrophotometer.

CHAPTER 4

RESULTS AND DISCUSSION

4.1. Characterization

4.1.1. XRD Measurements

Figure 4-1 shows XRD patterns of different samples (ZSM-5, SnO_2-ZSM-5, ZnO-ZSM-5, and TiO_2-ZSM-5). As indicated in Figure 4-1, all samples show the typical characteristic pattern of ZSM-5 phase [60], which means loading ZSM-5 with Sn, Zn, and Ti has no effect on its crystallinity. Furthermore, no diffraction peaks corresponding to SnO_2,ZnO, and TiO_2 indicating that either the loading level is low or the metal species (Sn, Zn, and Ti) are highly dispersed in ZSM-5. Note that the broad peak around 2θ = 12 degree of TiO_2-ZSM-5 spectrum is attributed to the holder of samples.

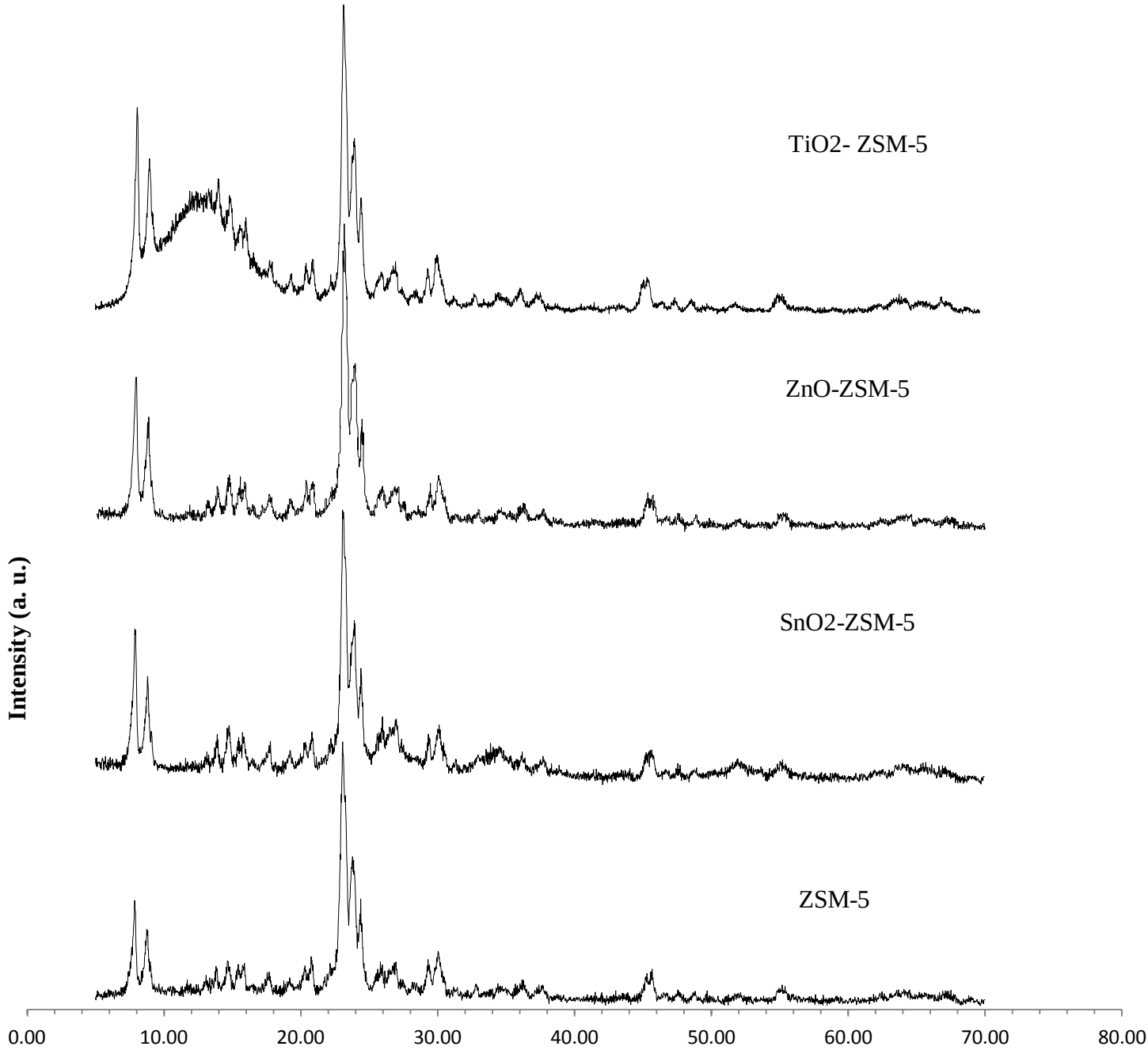

Figure 4-1 XRD pattern of synthesized materials

4.1.2. Fourier Transform Infrared Spectroscopy

Figure 4-2 shows FT-IR spectra of nano-sized TiO_2 −ZSM-5 (a), ZnO −ZSM-5 (b), ZSM-5 (c), and SnO_2-ZSM-5 (d). As indicated in Figure 4-2, spectrum (a) and spectra (b-d) show broad absorption bands at about 1622cm^{-1}, 3400 cm^{-1} and 3600 cm^{-1} belong to hydroxyl groups vibrations [22, 61, 62]. In addition, no absorption bands corresponding toTiO_2,ZnO and SnO_2 can be obviously observed in Figure 4-2. This can be attributed to the low level of metals or to the high dispersion of metal species (Ti, Zn, and Sn) in ZSM-5. As shown in Figure 4-2, the MFI of ZSM-5 phase is confirmed in the range 400-1300cm^{-1}. The band near 1222 cm^{-1} is assigned to the external asymmetric stretching vibrations of TO_4 (T= Si, Al) tetrahedral. In addition the adsorption band about at 1100 cm^{-1} is attributed to the internal asymmetric stretching vibration of Si-O-T. The bands near 550 and 790 cm^{-1} are attributed to double-five-member ring and internal tetrahedral TO_4 symmetric stretching vibrations respectively. The band at about 452 cm^{-1} belong to T-O bending vibration of AlO_4 and SiO_4 internal tetrahedral [20, 63].

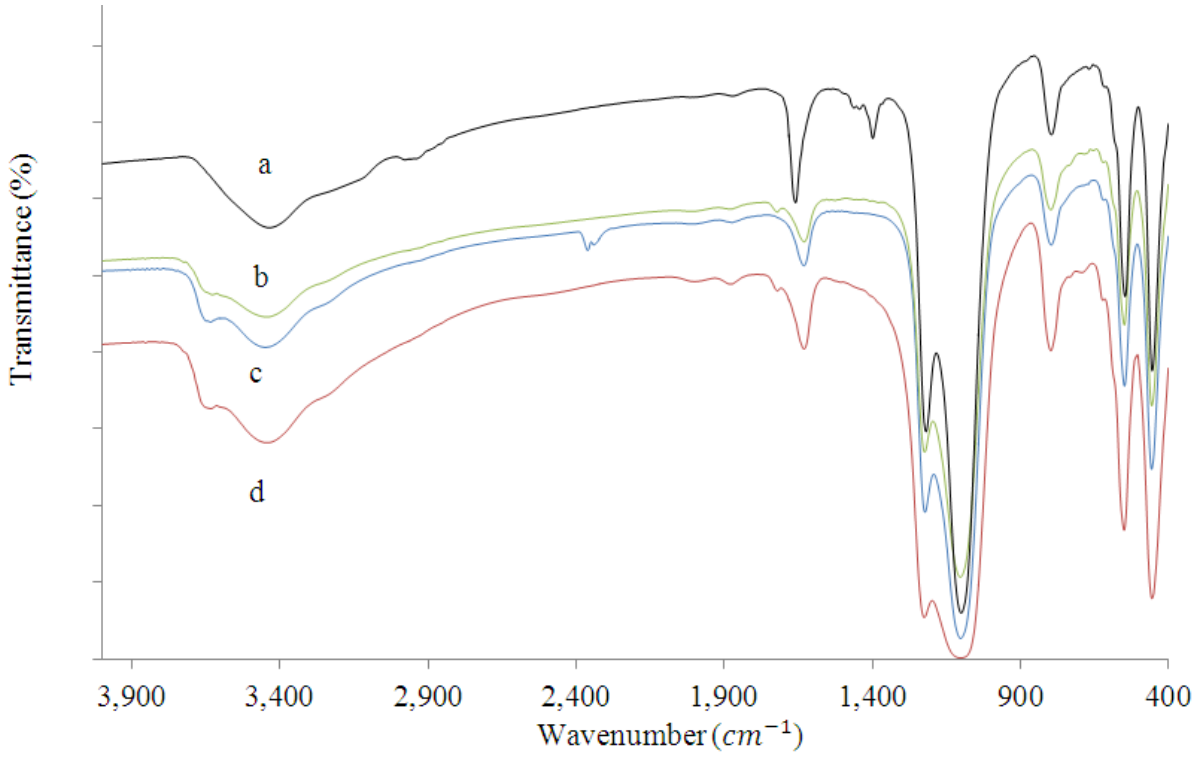

Figure 4-2 FTIR spectra of (a) TiO_2-ZSM 5, (b) ZnO-ZSM 5, (c) ZSM-5, and (d) SnO_2-ZSM-5

4.1.3. Morphology and EDS Characterization of Nano-Metal Oxide Zeolites

To study the morphology of the synthesized samples, a small quantity of the material was mixed with ethanol and ultra-sonicated for 5 minutes to reduce the aggregation of the particles. A drop of dispersed solution was deposited on a stub with copper conductive tape and dried and then coated with a gold layer to avoid the charging effect.

Figure 4-3 shows the morphology structure of ZSM 5, SnO_2-ZSM 5, ZnO-ZSM 5, and TiO_2-ZSM 5 samples. As illustrated in FESEM images, despite the agglomeration effect, a nanostructure nature of the synthesized materials is confirmed. It is seen on 500 nm scale bar nano-clusters with sub-structure around 40 nm (look at the center of the circles). In addition, the prepared materials seem to be porous at this scale.

Figure 4-4 shows EDS of the synthesized materials. As shown in Figure 4-4, the elemental compositions of ZSM 5 (Figure 4-4a) and the presence of metals (Sn, Zn, and Ti) in ZSM 5 structure (Figures 4-4b, 4-4c, and 4-4d) are confirmed.

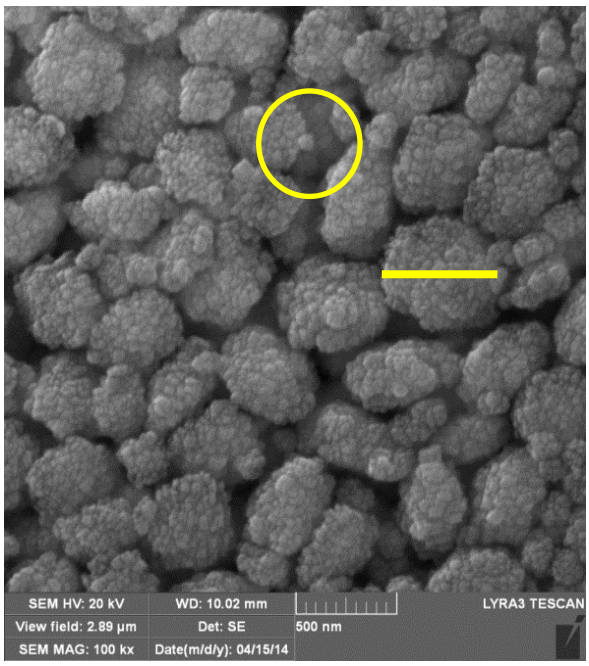

(a)

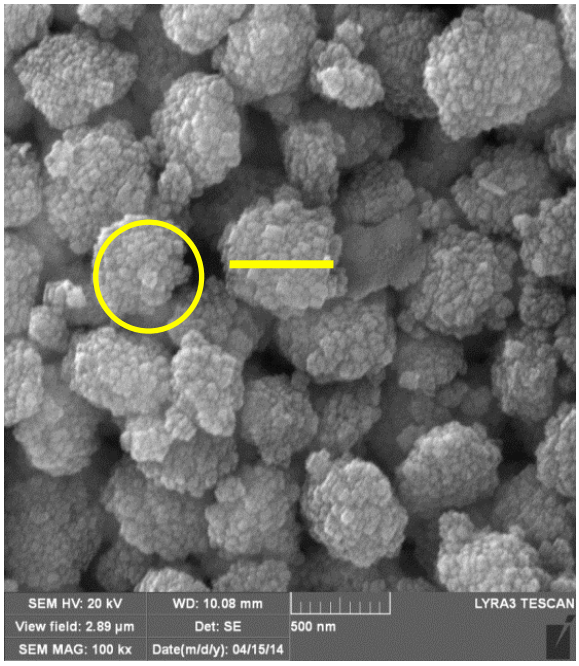

(b)

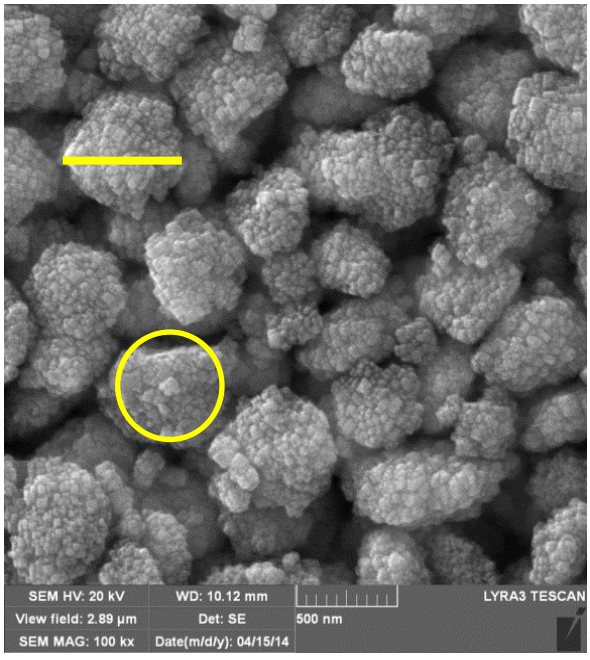

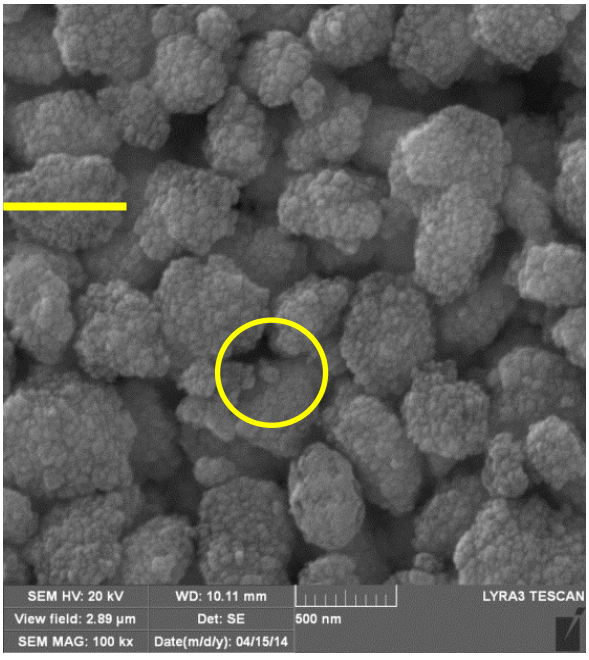

Figure 4-3 FESEM images at MAG. 100 kx of: (a) ZSM 5, (b) SnO_2-ZSM 5, (c) ZnO-ZSM 5, (d) TiO_2-ZSM 5

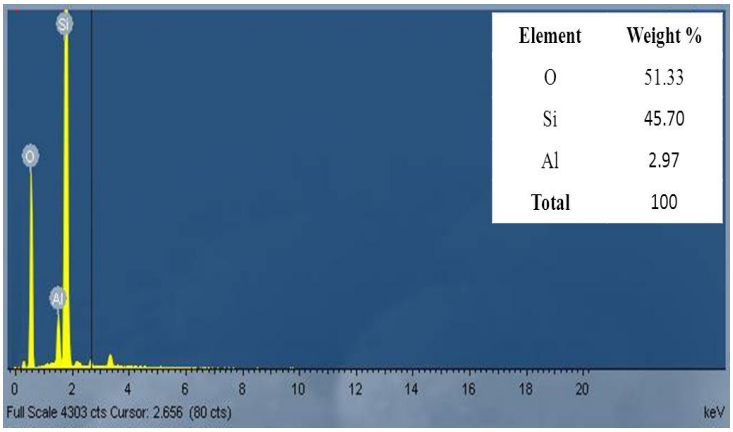

(a)

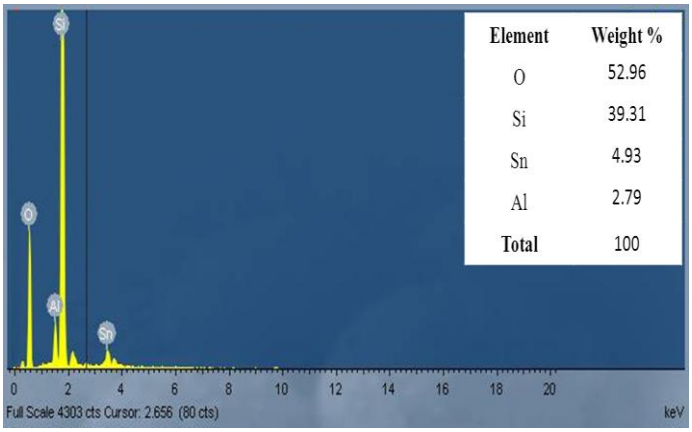

(b)

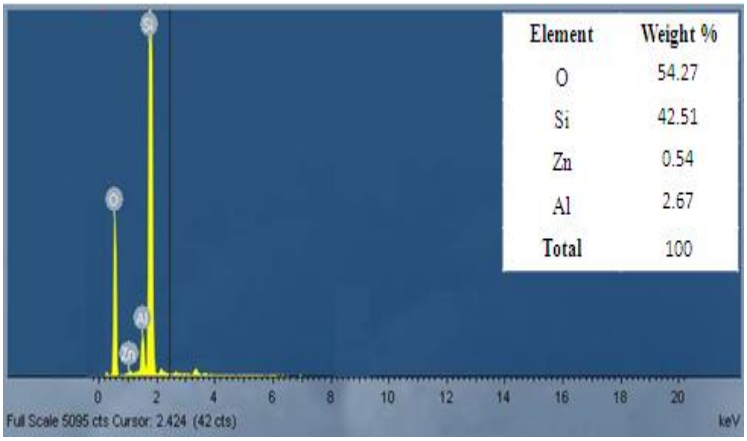

(c)

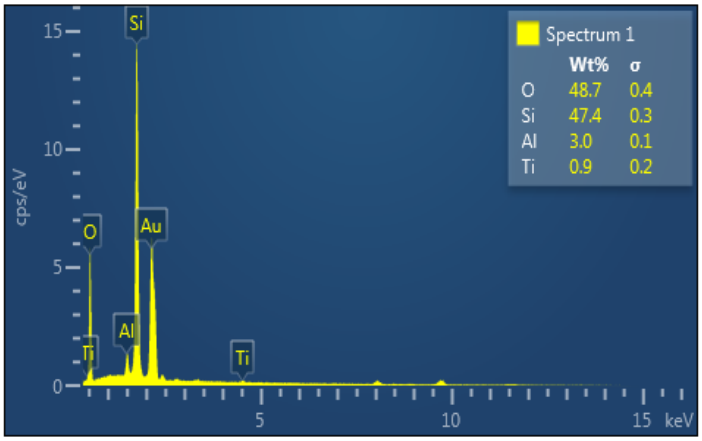

(d)

Figure 4-4 EDS spectra of: (a) ZSM 5, (b) SnO_2-ZSM 5, (c) ZnO-ZSM 5, (d) TiO_2-ZSM 5

4.1.4. HERTEM Characterization & Selected Area Electron Diffraction

The crystalline structure of the synthesized materials was further confirmed using HRTEM. Figure 4-5 show nano-crystals (approximately 40 nm in size) with well-defined inter spaces. In addition, HRTEM images confirmed the presence of nano-sized tin oxide (~5 nm) in ZSM 5, as shown in Figure 4-5b. The selected area electron diffraction also confirmed the crystallinity of the synthesized materials (see Figure 4-6).

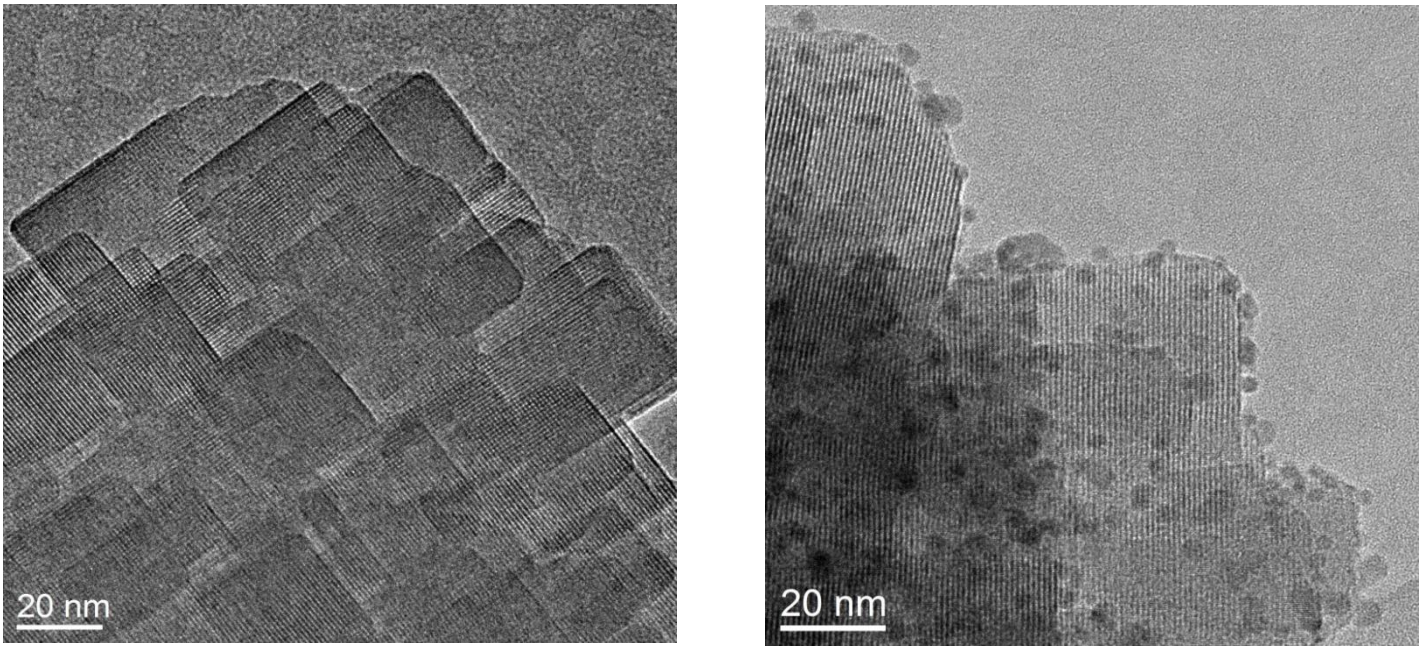

(a) **(b)**

Figure 4-5 HRTEM images of: (a) ZSM 5, (b) SnO_2-ZSM 5

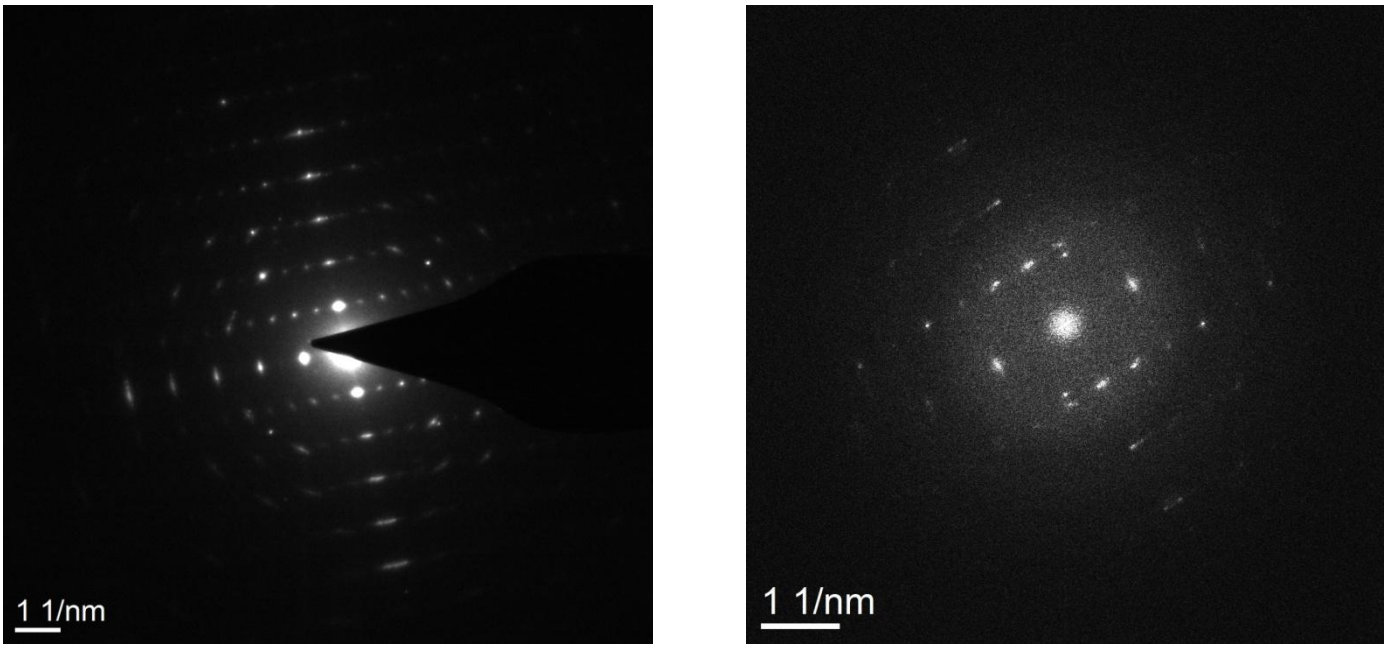

(a) **(b)**

Figure 4-6 Selected area electron diffraction of: (a) ZSM 5, (b) SnO_2-ZSM 5

4.1.5. XPS Analysis for Nano-Metal Oxide Zeolites

XPS analysis was carried out to get information about the elements present at the surface of the samples, and to determine oxidation states of the elements, In this analysis, a low-energy electron flood gun was used to neutralize the surface charging and the adventitious C1s peak was used to correct the small shift in binding energies due to surface charging.

As shown in the wide scan (Figure 4-7), O, Si, and Al were detected in ZSM 5 sample which confirm the elements of ZSM 5 [64].

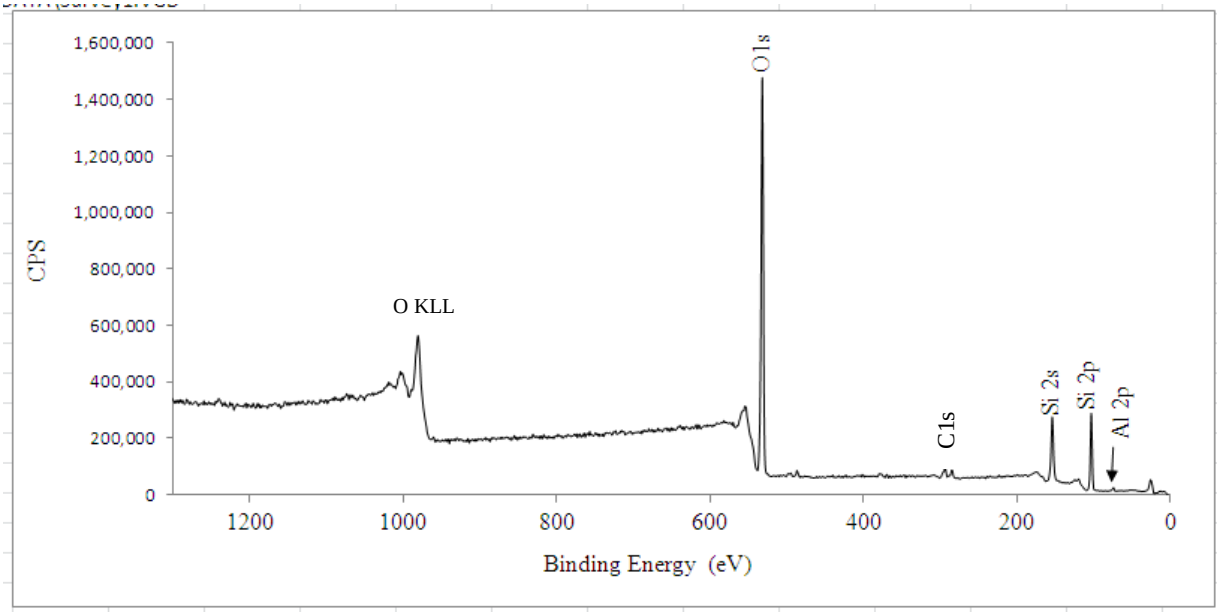

Figure 4-7 XPS survey spectrum of ZSM 5

Figure 4-8 shows the detailed spectra of O1s of ZSM 5, SnO_2-ZSM 5, ZnO-ZSM 5, and TiO_2-ZSM 5. According to the binding energy corresponding to the peaks, the oxidation state of oxygen is 2-. In addition, the small peaks at binding energies, around 534 eV and 529.4 eV, in Figures 4-8(a) and 4-8(b) could be attributed to adsorbed oxygen species on the surface due to the moisture and to the tin environment, respectively.

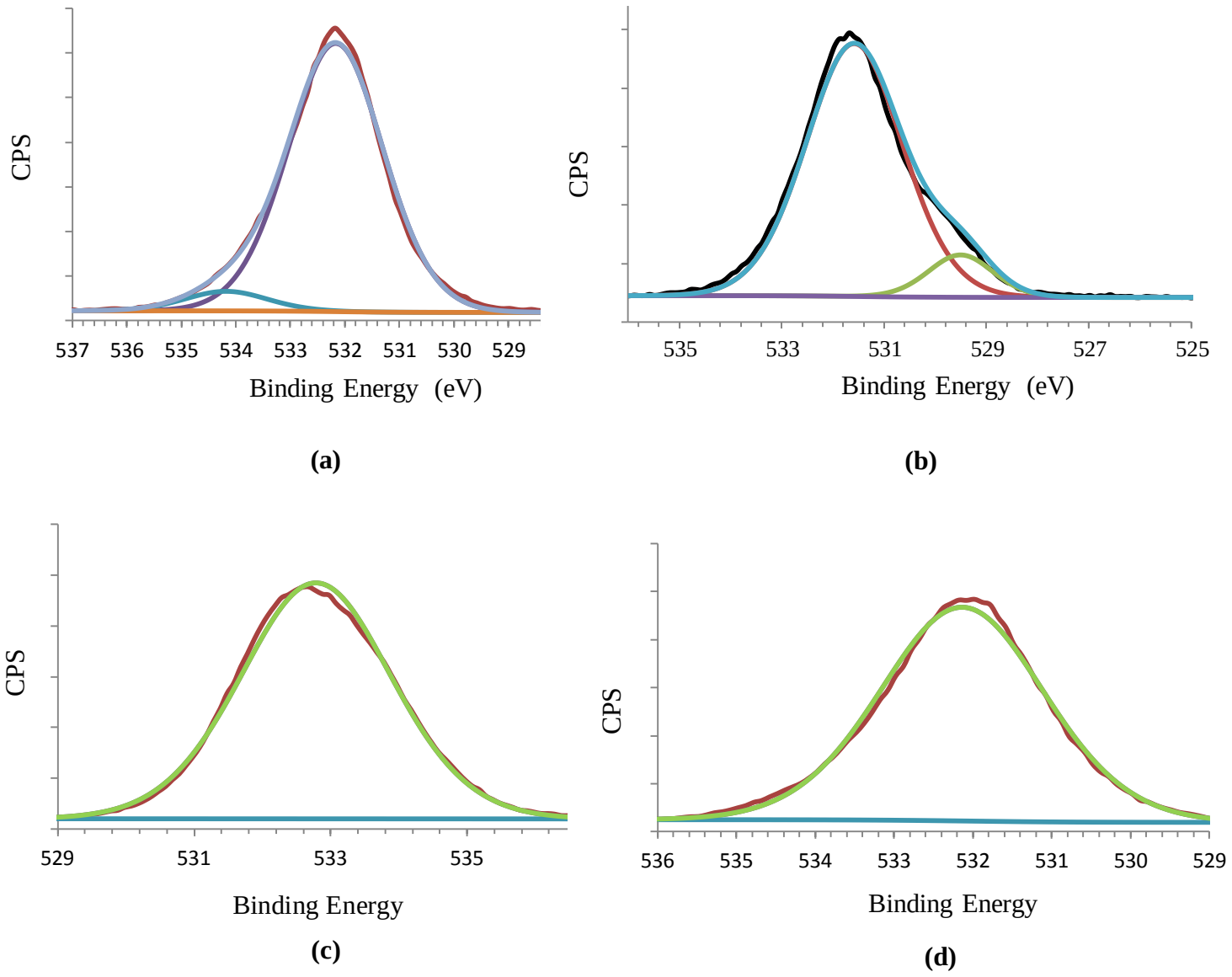

Figure 4-8 O1s peaks of XPS spectra of: (a) ZSM 5, (b) SnO_2-ZSM 5, (c) ZnO-ZSM 5, (d) TiO_2-ZSM 5

Figure 4-9 shows the detailed spectra of Al2p of ZSM 5, SnO_2-ZSM 5, ZnO-ZSM 5, and TiO_2-ZSM 5. According to the binding energy corresponding to the peaks, the oxidation state of aluminum is 3+.

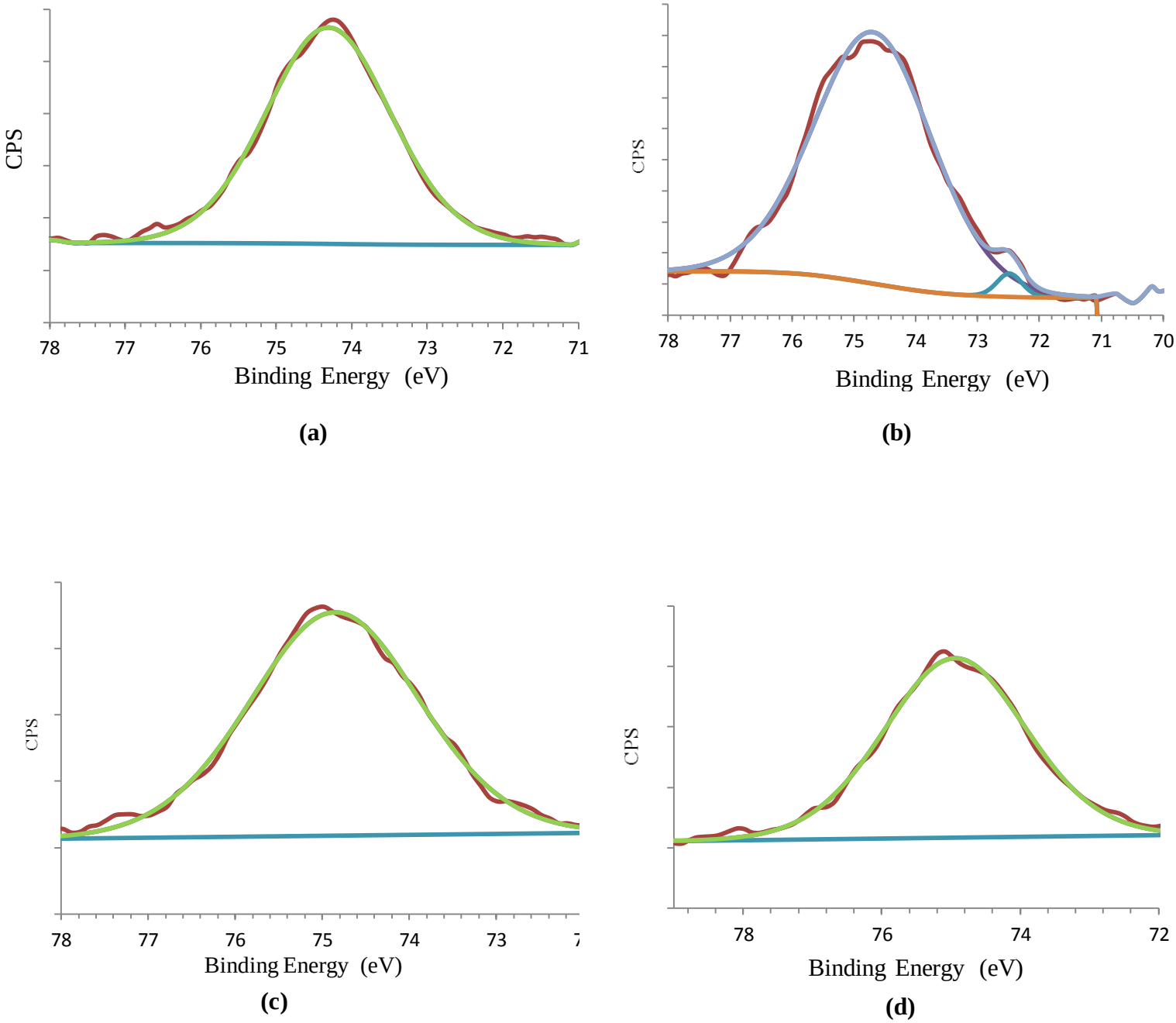

Figure 4-9 Al2p peaks of XPS spectra of: (a) ZSM 5, (b) SnO_2-ZSM 5, (c) ZnO-ZSM 5, (d) TiO_2-ZSM 5

Figure 4-10 shows the detailed spectra of Si2p of ZSM 5, SnO_2-ZSM 5, ZnO-ZSM 5, and TiO_2-ZSM 5. According to the binding energy corresponding to the peaks, the oxidation state of silicon is 4+. Furthermore, the peak around 102 eV in Figure 4-10b could be due to silicate.

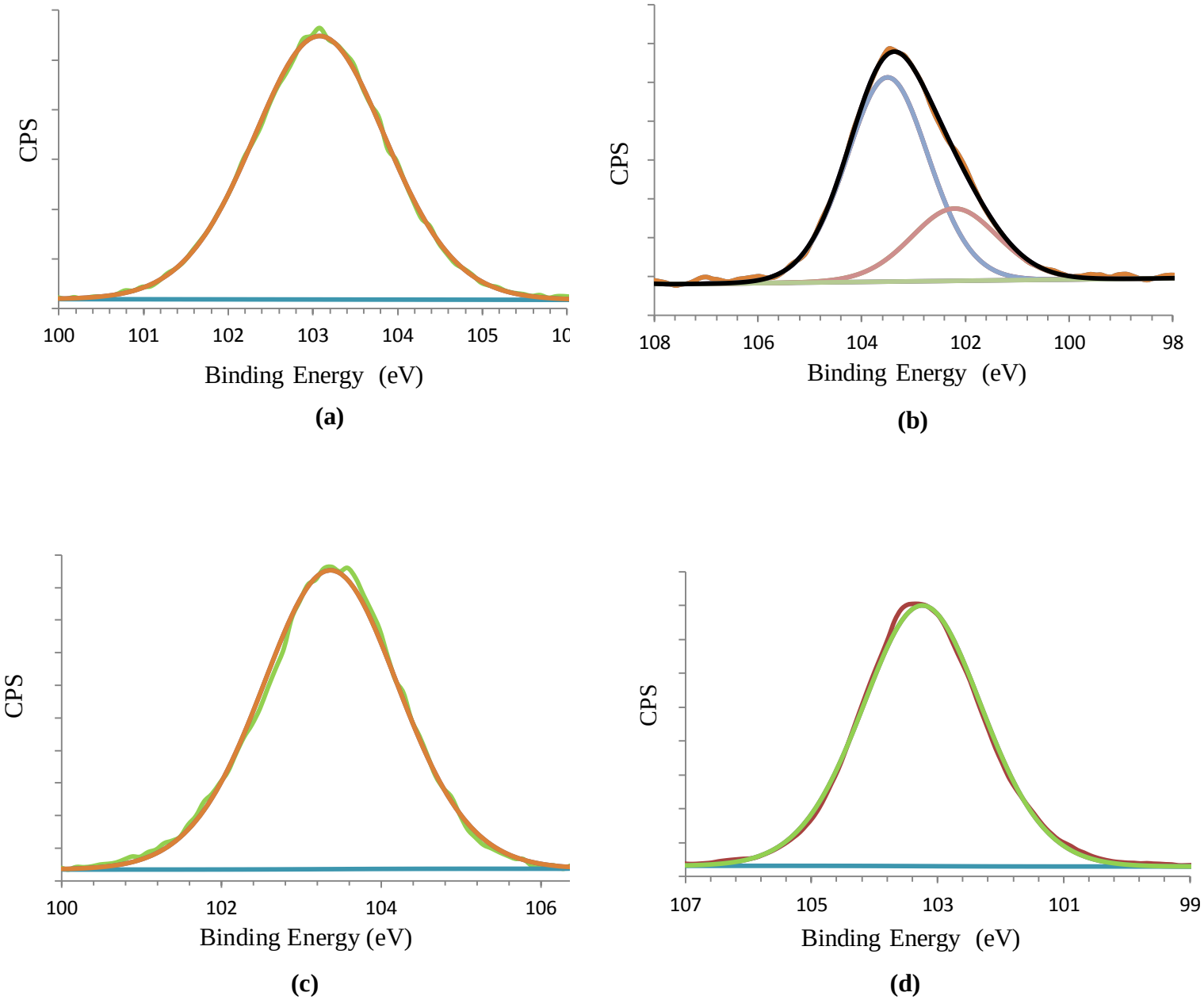

Figure 4-10 Si2p peaks of XPS spectra of: (a) ZSM 5, (b) SnO_2-ZSM 5, (c) ZnO-ZSM 5, (d) TiO_2-ZSM 5

Figure 4-11 shows the detailed spectra of Sn3d5/2, Zn2p3/2, and Ti2p3/2 of SnO_2-ZSM 5, ZnO-ZSM 5, and TiO_2-ZSM 5, respectively. According to the binding energies corresponding to the peaks, the oxidation state of Sn, Zn, and Ti are 4+, 2+, and 4+, respectively.

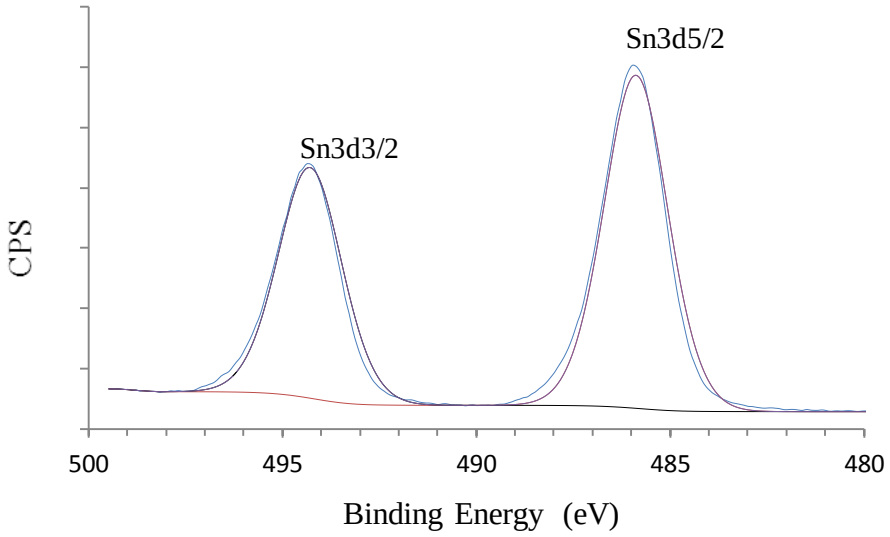

(a)

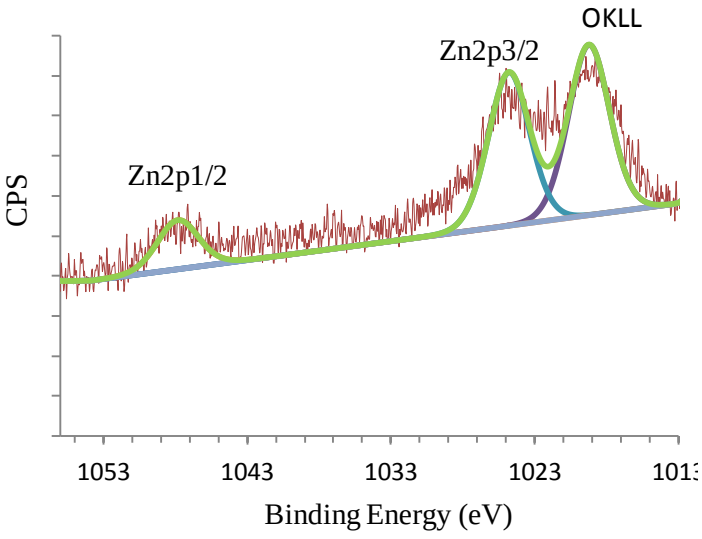

(b)

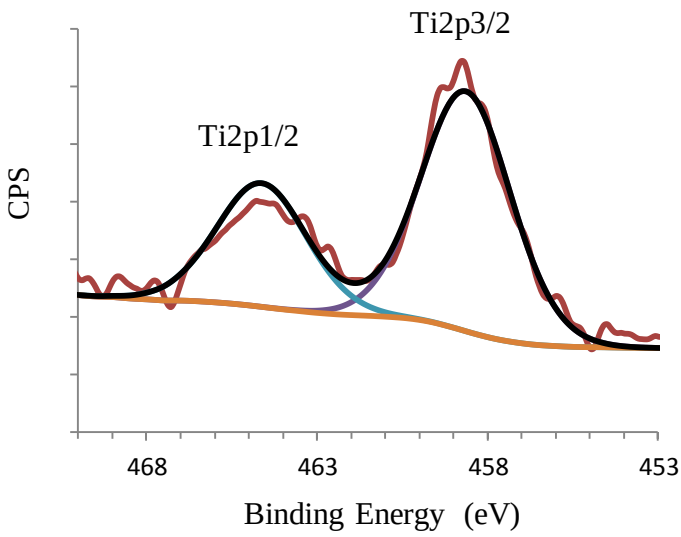

(c)

Figure 4-11: (a) Sn3d5/2 and Sn3d3/2 peaks of XPS spectrum of SnO_2-ZSM 5, (b) Zn2p3/2 and Zn2p1/2 peaks of XPS spectrum of ZnO-ZSM 5, (c) Ti2p3/2 and Ti2p1/2 peaks of XPS spectrum of TiO_2-ZSM 5.

4.2. Nano-Metal Oxide Zeolites for Hydrogen Gas Detection

4.2.1. Hydrogen Gas Sensing System

Hydrogen gas sensing system is depicted in Figure 4-12(a-c). As shown, two cylinders (dry nitrogen and 10000 ppm hydrogen in dry nitrogen) are stored in the container. The sensor is placed on a stage (see Figure 4-12a) and connected to a semiconductor device analyzer (SDA) through two electrodes (as seen in Figure 4-12b) for electrical conductivity measurements. A water cooling system is connected to the measurement stage to keep it cool while a heater raises the temperature of the block under the sensor. The measurement stage inlet is connected to a gas line and its outlet is connected to the laboratory exhaust. Dry nitrogen and hydrogen Mass Flow Controllers (MFCs) are used for diluting the target gas (hydrogen). The electrical conductivity of the sensor is measured at different temperatures, and at different concentrations of hydrogen.

a)

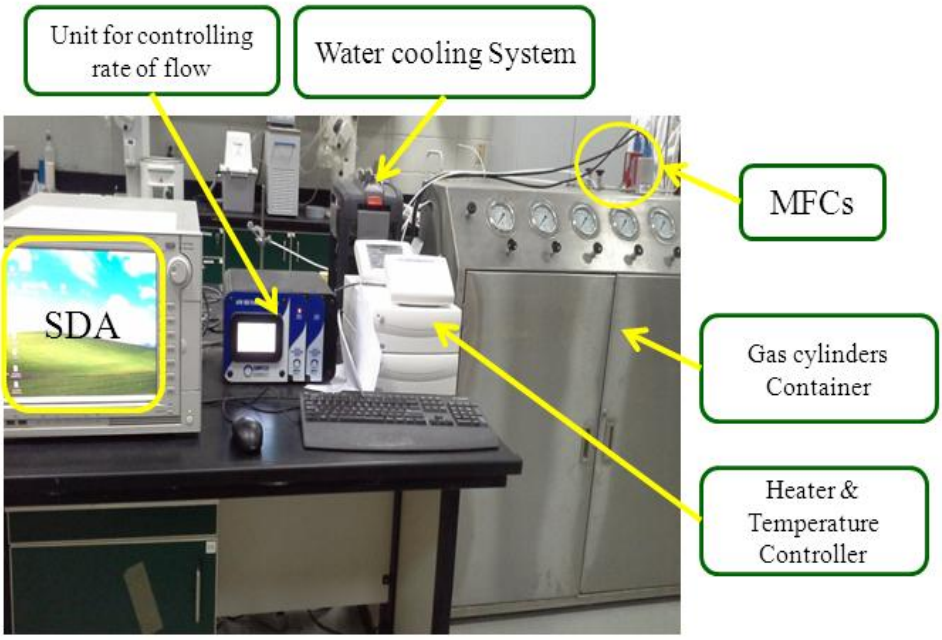

b)

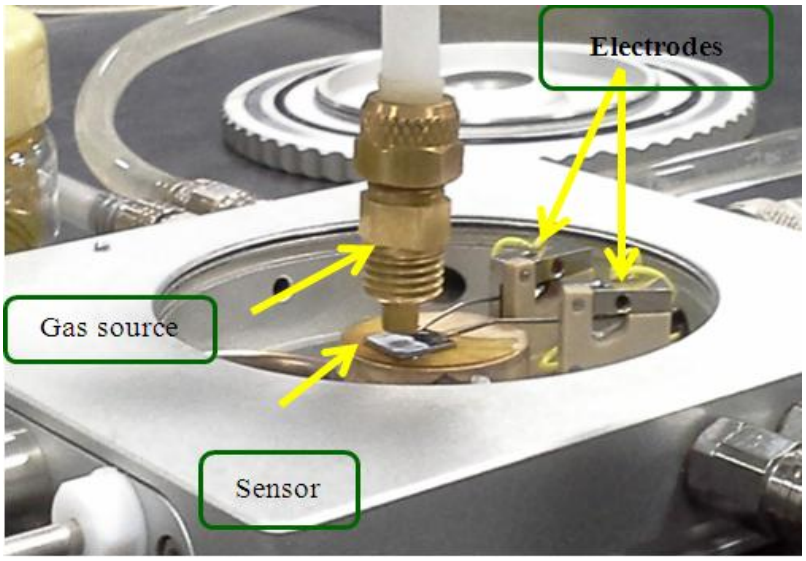

c)

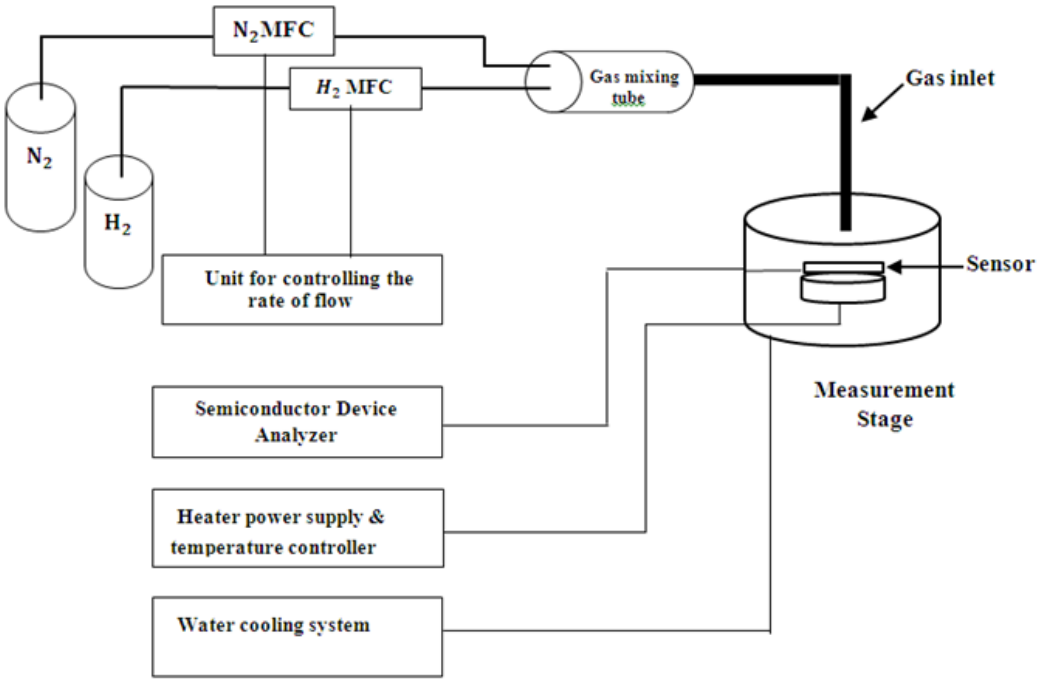

Figure 4-12 Hydrogen gas sensing measurements system: a) A photo of the whole system, CENT, KFUPM, b) A sensor placed in a measurement stage, c) Schematic diagram of the experimental set-up of hydrogen gas measurements.

4.2.2. Sensor Fabrication

Our hydrogen gas sensor belongs to chemiresistor gas sensor type, explained in section 1.2. It is composed of interdigitated electrodes (IDE) sputtered on a silicon dioxide isolation layer grown on a silicon substrate. The synthesized metal oxide zeolites are brushed on the IDE as a thick film.

The IDE was a pair of 11 fingers; each electrode was 100 micron wide with 100 micron spacing to its neighboring electrodes. The electrodes were 200 nano-meters thick (see Figure 4-13a).

Few milligrams of nano-metal oxide zeolites (ZnO-ZSM5, SnO2-ZSM5, and TiO2-ZSM5) were mixed in few milliliters of ethanol. The mixture was ultra-sonicated for 10 minutes to achieve dispersion and then applied on IDEs (see Figure 4-13b).

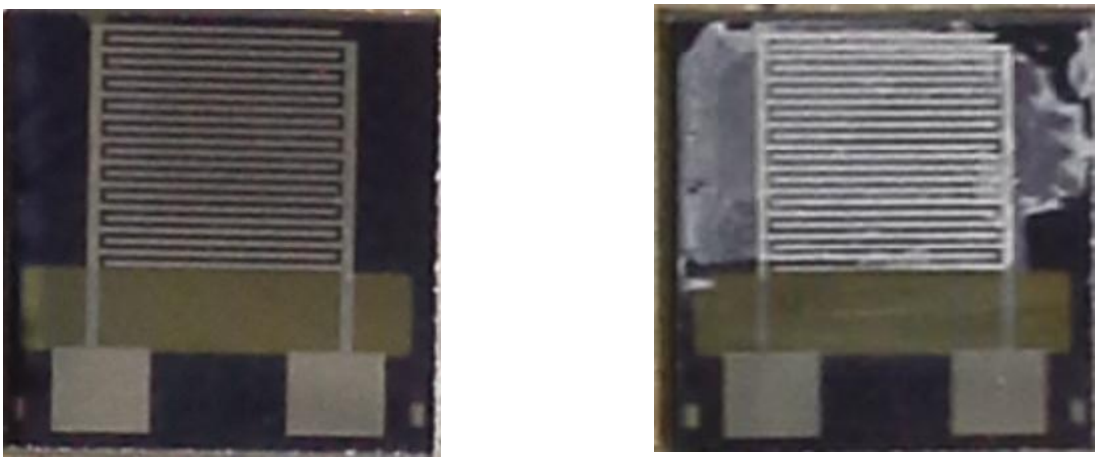

(a) **(b)**

Figure 4-13 Interdigitated electrodes: a) Before applying the sensing material, b) After applying the sensing material

.

4.2.3. Hydrogen Gas Measurements

Prior to hydrogen gas measurements, dry nitrogen gas at rate of flow 20SCCM (Standard Cubic Centimeter per Minute) was kept constant for 30 minutes during stabilization of the elevated temperatures. Dry nitrogen gas was used as the reference gas throughout our hydrogen gas measurements. The concentration of hydrogen is presented in ppm (parts per million) units, indicating the number of hydrogen particles per total number of particles in mixture. In our study, the concentration of hydrogen gas in a balance gas (nitrogen) is 1 % (10000ppm). However, the total flow rate of dry nitrogen and hydrogen mixture was fixed at 20 SCCM and the concentration of hydrogen was varied according to this formula:

$$H_{2\ Conc.} = H_2^{/} \left(\frac{QH_2}{QH_2 + QN_2}\right)$$

where $H_2^{/}$ is the concentration of hydrogen inside the cylinder (10000ppm), QH_2 is the flow rate of hydrogen with 10000ppm, and QN_2 is the flow rate dry nitrogen. Since the total flow rate was fixed at 20 SCCM and by using Eq. 1, the hydrogen concentration can be varied. The sensor response is defined as the relative change in the resistance of the sensor:

$$Response(\%) = \left(\frac{R_{air} - R_{gas}}{R_{air}}\right) \times 100$$

As illustrated in figures 4-14 to 4-19, ZnO-ZSM 5, SnO_2-ZSM 5, and TiO_2-ZSM 5. Sensors show response to different concentrations of hydrogen at operating temperatures of 300 and 350℃. The sensing behavior noticed here could be attributed to the metal oxides (ZnO, SnO_2, and TiO_2) which are n-type semiconductors.

The sensing mechanism is complicated. Yet, it is commonly accepted that the mechanism is considered as a surface effect in which the conductivity of the sensing material is changed due to adsorption and chemical reactions taking place on the surface of the sensing material.The response noticed in figures 4-28 to 4-33 can be explained according to the following reactions:

In the first reaction, atmospheric oxygen is adsorbed on the surface of n-type semiconductor materials (ZnO, SnO_2, and TiO_2) in the form of $O_2^-, O^- and O^{2-}$ (depending on operating temperatures) which results in consuming of electrons [3, 18]:

$$O_{2(gas)} + 2e^- \leftrightarrow 2O^-_{(ads)}$$

The trapping of electrons from the surface causes decreasing in the conductivity of n-type semiconductor which form a depletion region. In the second reaction, introducing the reducing gas (H_2), desorbs the adsorbed oxygen according to the following equation:

$$H_{2(gas)} + O^-_{(ads)} \rightarrow H_2O + e^-$$

resulting in releasing the trapped electrons to conduction band, and then increasing in the conductivity of the semiconductor. Thus, the concentrations of oxidizing or reducing gases can be measured by monitoring the changes in the conductivity of semiconducting materials.

4.2.3.1. Sensing Performance of Nano Metal Oxide-ZSM 5

Figure 4-15a shows the gas response of ZnO-ZSM 5 to 0.2%, 0.4%, 0.6, and 1% of hydrogen gas at 350℃. As shown, the response increases with increasing hydrogen concentration. In addition the gas response of ZnO-ZSM 5 at small concentrations (0.05%, 0.1%, 0.15%, and 0.2%) and at different temperatures (300℃ and at 350℃) was measured (see Figure 4-15b and Figure 4-15c). As shown in Figure 4-15(b &c), there is small increase in the sensor response with increasing the concentration of hydrogen. On the other hand, the sensor response at 300℃ is almost the same as at 350℃. Figure 4-16 shows a non-cyclic response of ZnO-ZSM 5 to 0.1%, 0.2%, 0.3%, 0.4%, and 0.5% of hydrogen at 350℃. As seen, the response as a function of hydrogen concentration is almost linear, which is a good property compared to pure metal oxide sensors that show non-linear relation in this range of concentrations.

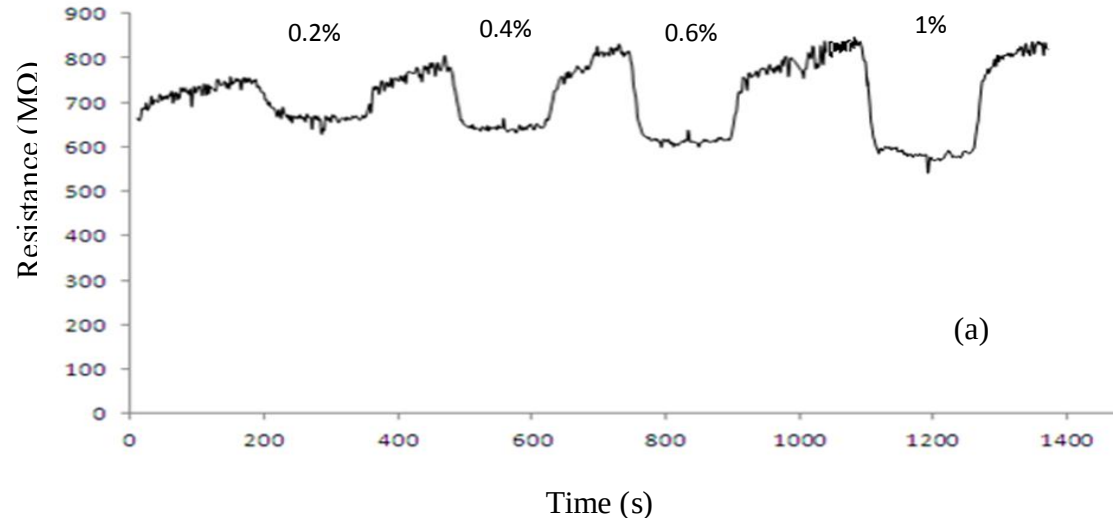
0.2%
0.4%
0.6%
1%
Resistance (MΩ)
900
800
700
600
500
400
300
200
100
0
0
200
400
600
800
1000
1200
1400
(a)
Time (s)

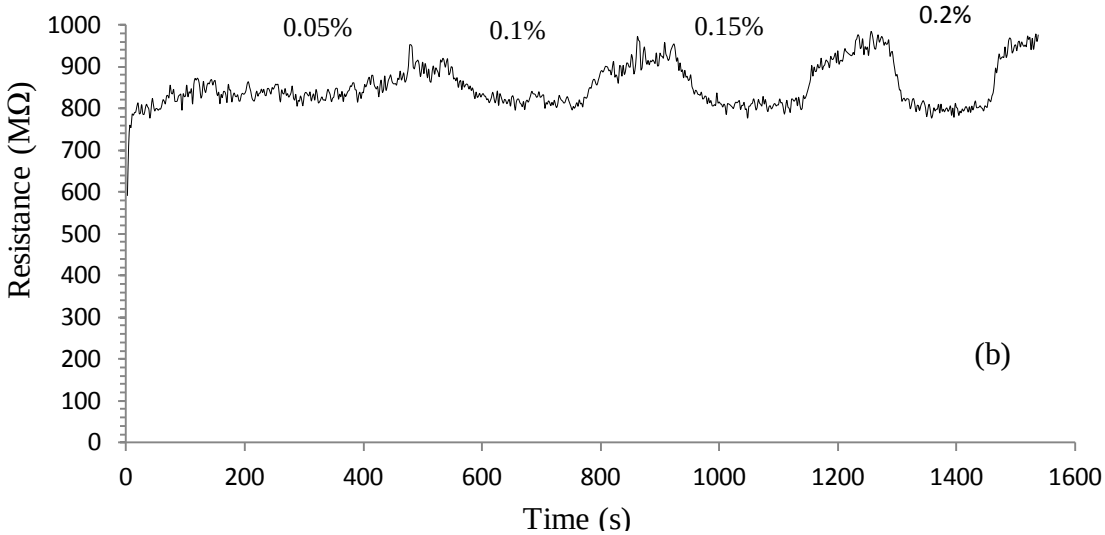
0.05%
0.1%
0.15%
0.2%
Resistance (MΩ)
1000
900
800
700
600
500
400
300
200
100
0
0
200
400
600
800
1000
1200
1400
1600
(b)
Time (s)

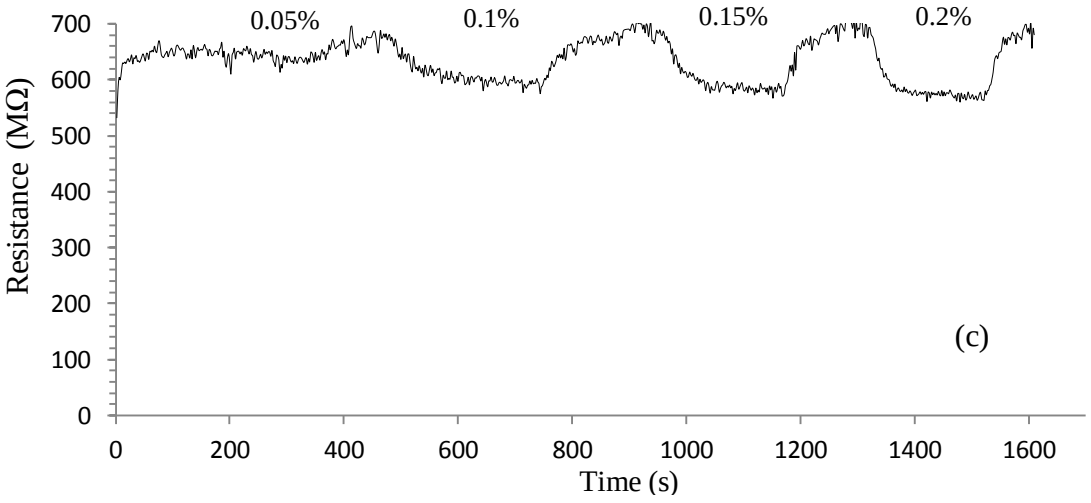

Figure 4-14 Gas response of ZnO-ZSM 5 sensor to different concentrations of H_2 (as labelled) at 350℃ (a) & (b), and at 300℃(c)

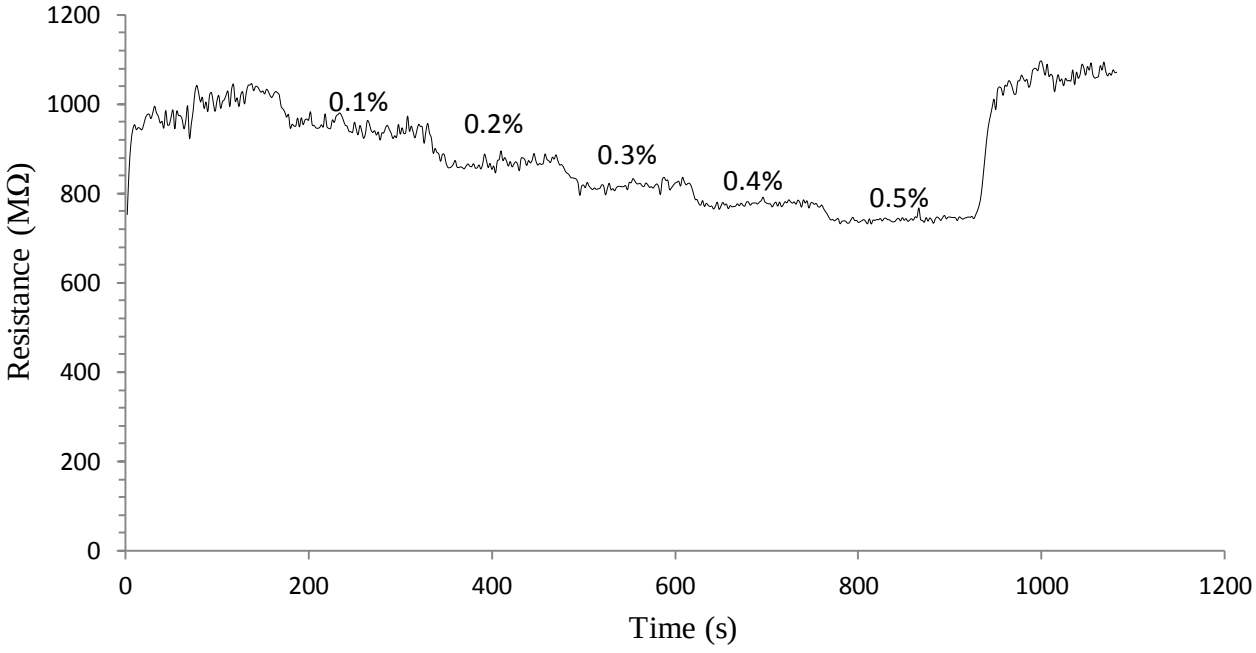

Figure 4-15 Gas response of ZnO-ZSM 5 sensor to different concentrations of H_2 (as labelled) at 350℃

SnO_2-ZSM5 and TiO_2-ZSM5 based sensors (see Figures 4-17 to 4-20) showed similar behavior to ZnO-ZSM 5 based sensor with exception that the responses ofSnO_2-ZSM5 and TiO_2-ZSM5 based sensors are weak compared to the response of ZnO-ZSM 5 based sensor. In addition, the response times of ZnO-ZSM 5, TiO_2-ZSM 5 and SnO_2-ZSM 5 were measured at hydrogen concentration of 1% and they are, approximately, 20s, 34s and 30s, whereas the recovery times are 54s, 64s and 70s, respectively.

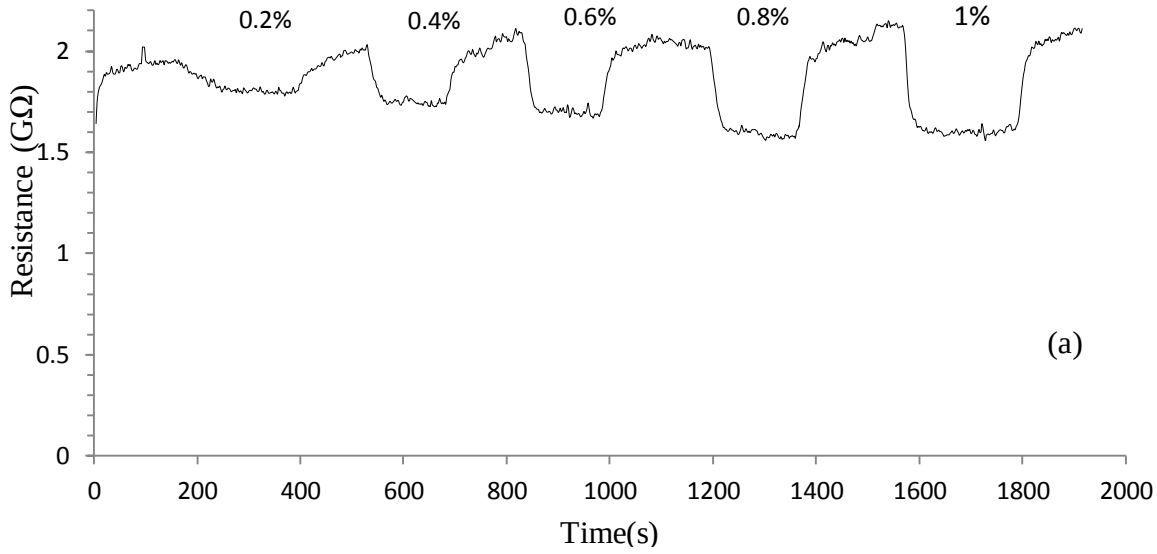

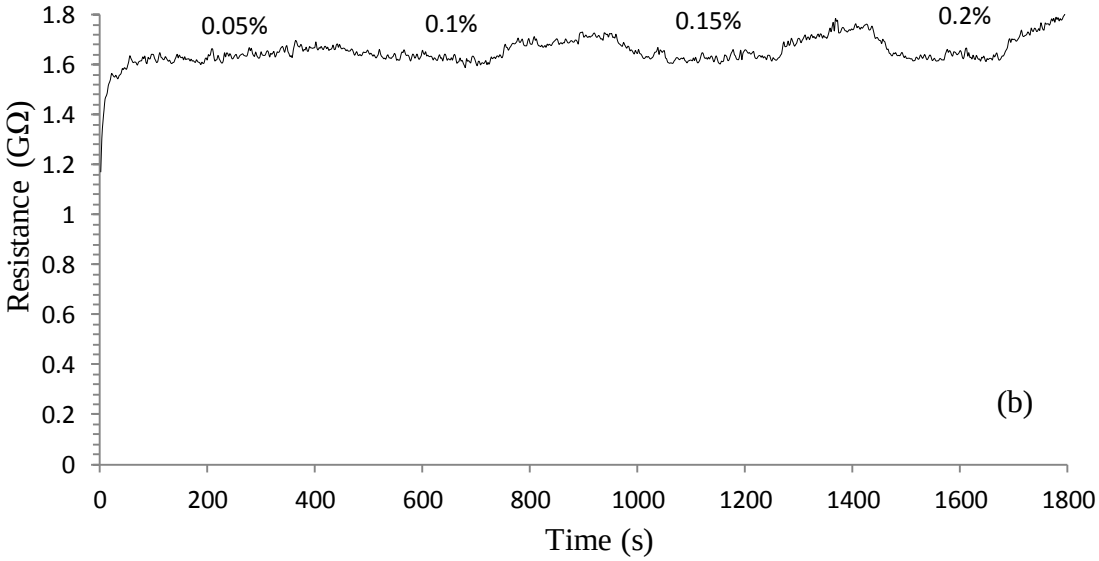

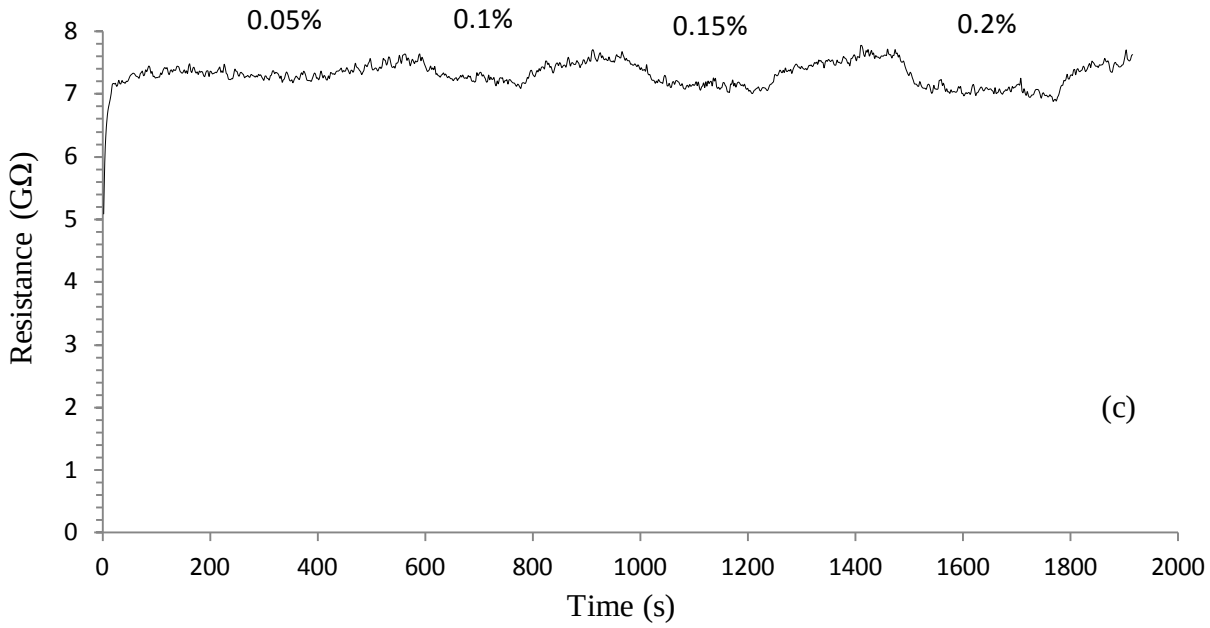

Figure 4-17 Gas response of SnO2-ZSM 5 sensor to different concentrations of H_2 (as labelled) at 350℃

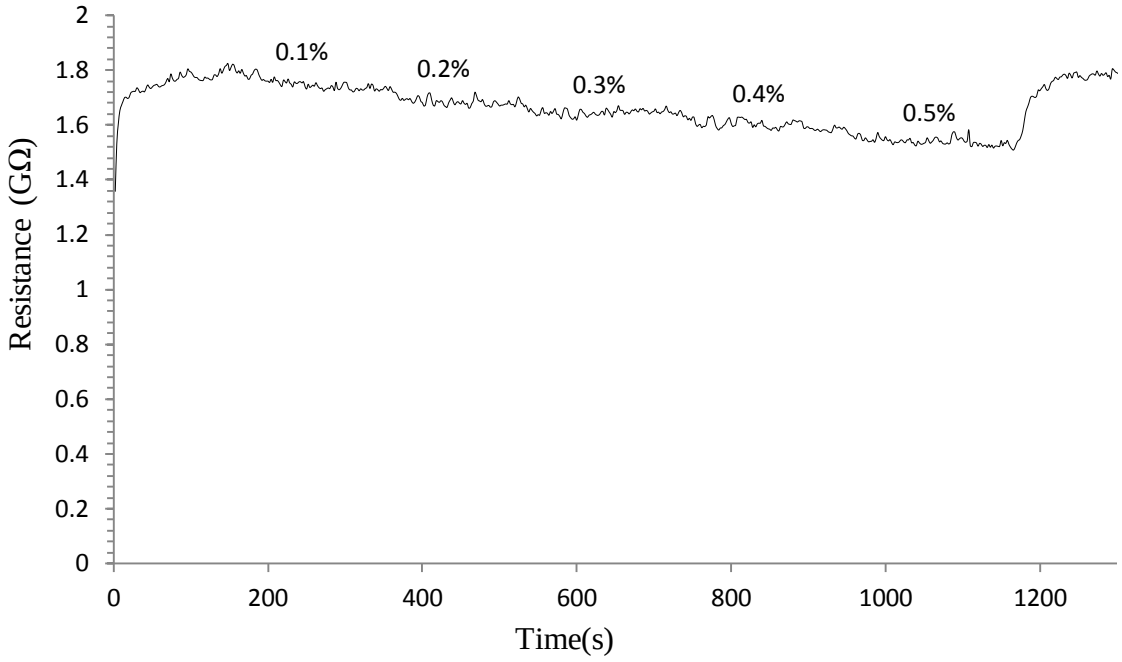

Figure 4-16 Gas response of SnO2-ZSM 5 sensor to different concentrations of H_2 (as labelled) at 350℃ (a) & (b) and at 350℃ (c)

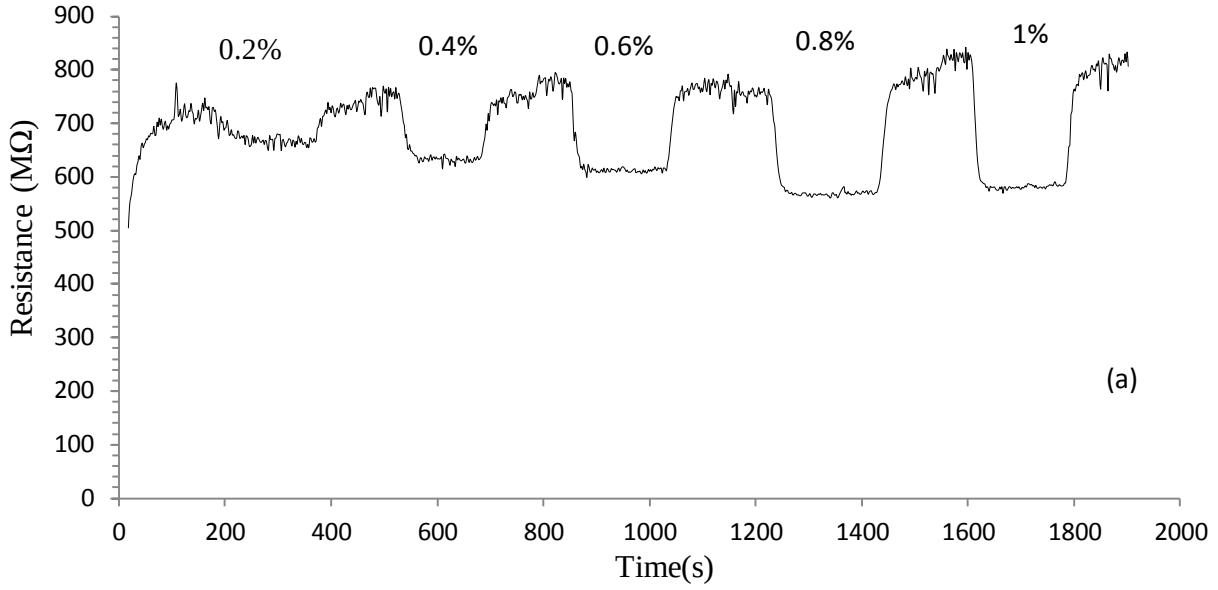
0.2%
0.4%
0.6%
0.8%
1%
Resistance (MΩ)
Time(s)
(a)

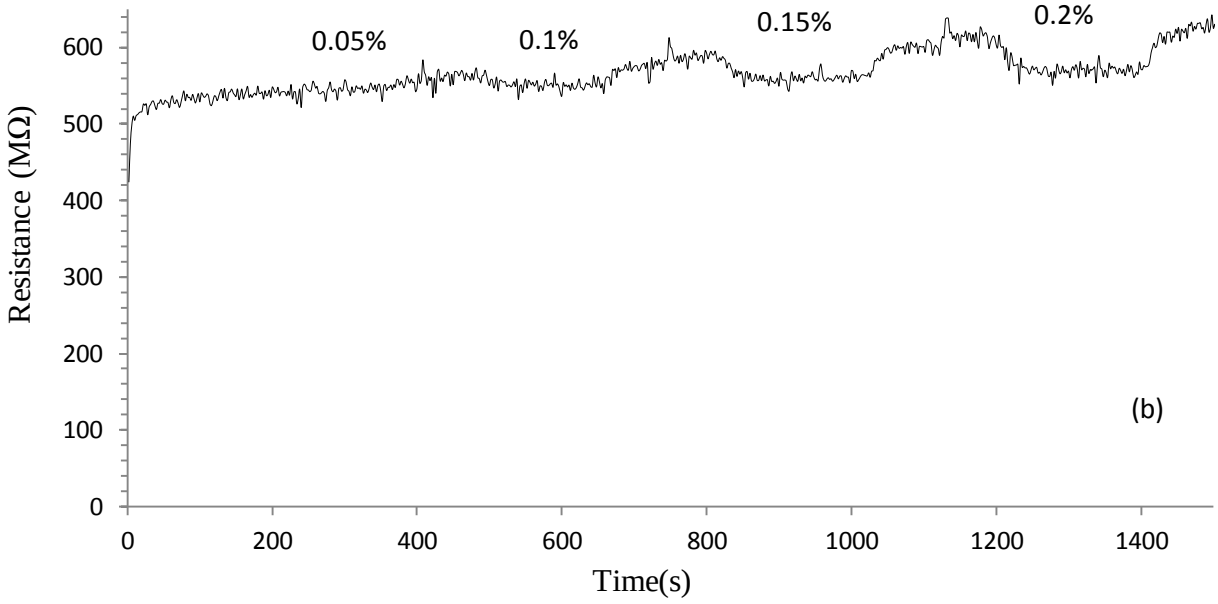
0.05%
0.1%
0.15%
0.2%
Resistance (MΩ)
Time(s)
(b)

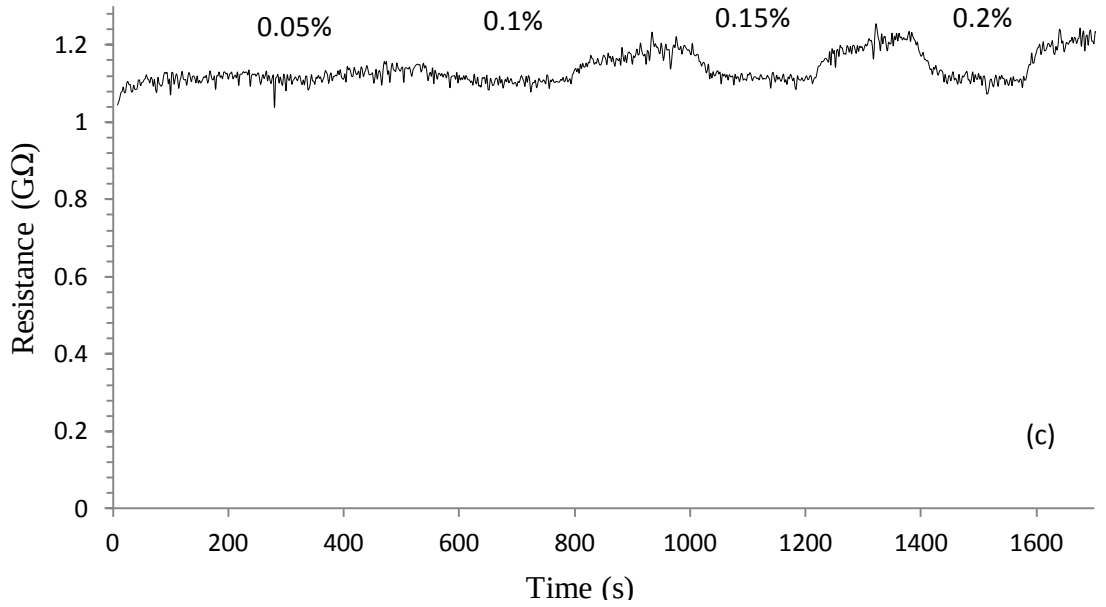

Figure 4-18 Gas response of TiO2-ZSM 5 sensor to different concentrations of H_2 (as labelled) at 350℃ (a) & (b) and at) at 300℃ (c)

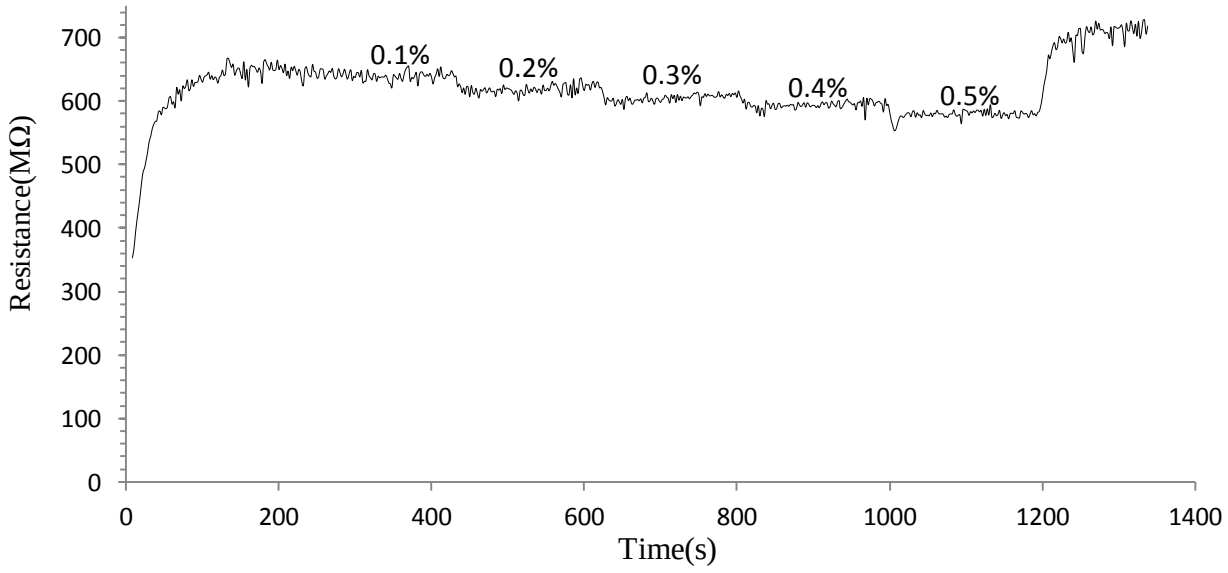

Figure 4-19 Gas response of TiO2-ZSM 5 sensor to different concentrations of H_2 (as labelled) at 350℃

Figure 4-20 shows the response of ZnO-ZSM 5, TiO_2-ZSM 5 and SnO_2-ZSM 5 as a function of hydrogen concentrations at 350℃. As shown, ZnO-ZSM 5 sensor has the highest response, while SnO_2- ZSM 5 sensor has the lowest response. In addition, the operating ranges of ZnO-ZSM 5,TiO_2-ZSM 5 and SnO_2-ZSM 5 based sensors seem to be linear in the range between 0.2% and 1%, with $R^2 = 0.9817, 0.9923,$ and 0.9547 of ZnO-ZSM 5,TiO_2-ZSM 5 and SnO_2-ZSM 5 respectively. The high response of ZnO-ZSM 5 based sensor could be attributed to the high dispersion of ZnO in ZSM 5.

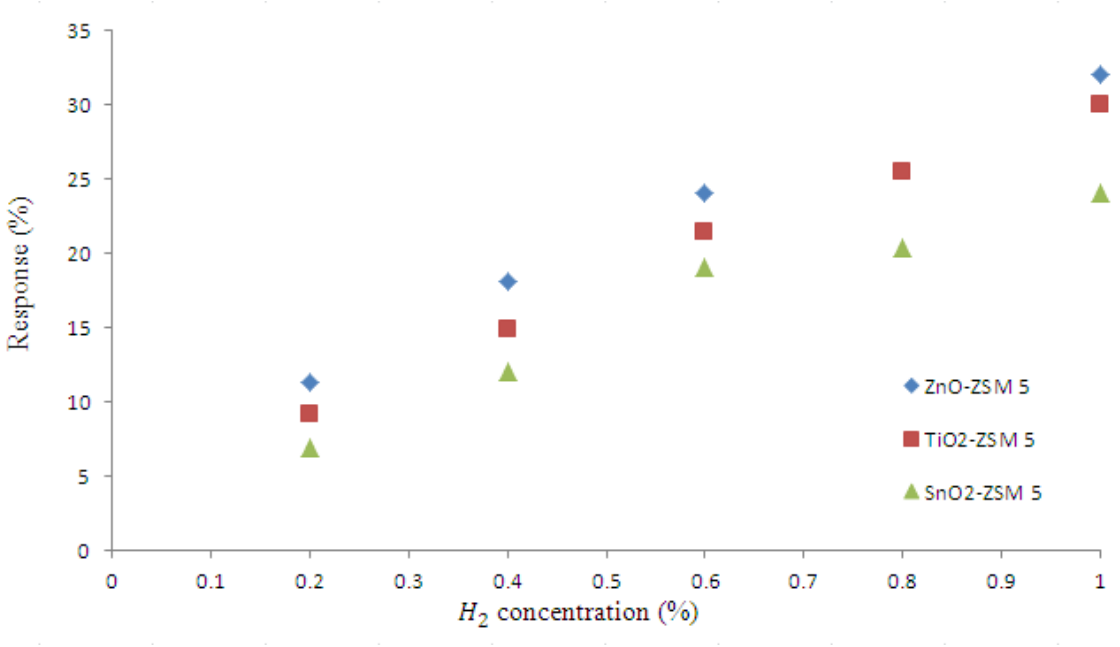

Figure 4-20 Response versus concentrations of H_2: ZnO-ZSM 5, TiO2-ZSM 5, SnO2-ZSM 5 at 350℃.

CHAPTER 5

CONCLUSION

In this study, nanocrystalline ZSM 5, ZnO-ZSM 5, SnO_2-ZSM 5, and TiO_2-ZSM 5 materials were synthesized and characterized using XRD, FTIR, FESEM, HRTEM, EDS, and XPS techniques. The crystallinity of the synthesized materials was confirmed by XRD and by selected area electron diffraction achieved by HRTEM. No diffraction peaks corresponding to metal oxides (ZnO, SnO_2, and TiO_2) were noticed in XRD spectra. This is probably related to the low loading level of the metal species as well as its high dispersion. Furthermore, FTIR spectra confirmed zeolitic structures. The morphology and size of the synthesized materials were investigated using FESEM. The nanostructured nature of prepared materials with nano-clusters shapes was confirmed. In addition, HRTEM was used to confirm the nano-crystalline structure of the synthesized materials, where nano-crystals with size approximately around 40 nm were observed. HRTEM images confirmed the presence of nano-sized metal species (~5 nm) in ZSM 5

EDS and XPS analyses confirmed the presence of metal species in the synthesized samples. Furthermore, the oxidation states of elements were investigated using XPS.

In terms of sensing properties , ZnO-ZSM 5, SnO_2-ZSM 5, and TiO_2-ZSM 5 samples showed acceptable response to hydrogen gas at different concentrations (0.05%, 0.1%, 0.2%, 0.4%, 0.6%, 0.8%, and 1%) and different operating temperatures (300℃ and 350℃). The response of ZnO-ZSM 5, SnO_2-ZSM 5, and TiO_2-ZSM 5-based sensors at 300℃ and 350℃ was approximately similar. On the other hand, the response of ZnO-ZSM 5,TiO_2-ZSM 5 and SnO_2-ZSM 5-based sensors as a function of hydrogen concentration is approximately linear in the range between 0.2% and 1%, with $R^2 = 0.9817, 0.9923,$ and 0.9547 of ZnO-ZSM 5,TiO_2-ZSM 5 and SnO_2-ZSM 5 respectively. ZnO-ZSM 5-based sensor showed the highest response, while SnO2-ZSM 5-based sensor showed the lowest response. The high response of ZnO-ZSM 5 is probably related to the high dispersion of zinc species in ZSM 5. In addition, the response times of ZnO-ZSM 5, TiO_2-ZSM 5 and SnO_2-ZSM 5 were measured at concentration 1% of hydrogen and they are, approximately, 20s, 34s and 30s, whereas the recovery times are 54s, 64s and 70s, respectively. In future work, we will test the selectivity of the nano metal oxide zeolites for different gases. Also we will try to improve on the sensitivity of the material while retaining linear response, and improve on the sensitivity of the material while retaining linear response.

References

[1] Retrieved from http://www.esrl.noaa.gov/gmd/ccgg/trends/

[2] Retrieved from http://www.inspectapedia.com/

[3] Korotchenkov, GennadiĭSergeevich. *Handbook of Gas Sensor Materials: Properties, Advantages and Shortcomings for Applications Volume 1: Conventional Approaches*. Vol. 1. Springer, 2013.

[4] Aswal, Dinesh K., and Shiv K. Gupta, eds. *Science and technology of chemiresistor gas sensors*. Nova Publishers, 2007.

[5] Brattain, W. H., and C. G. B. Garrett. "Surface Properties of Germanium and Silicon." *Annals of the New York Academy of Sciences* 58.6 (1954): 951-958.

[6] Seiyama, Tetsuro, et al. "A New Detector for Gaseous Components UsingSemiconductive Thin Films." *Analytical Chemistry* 34.11 (1962): 1502-1503.

[7] N. Taguchi, published patent application in Japan, S37-47677, Oct. 1962

[8] Iftimie, N., et al. "Gas sensitivity of nanocrystalline nickel ferrite." *Journal of Optoelectronics and Advanced Materials* 8.3 (2006): 1016.

[9] Sandu, Izabela, et al. "Nanostructured cobalt manganese ferrite thin films for gas sensor application." *Thin Solid Films* 495.1 (2006): 130-133.

[10] Gadkari, Ashok B., Tukaram J. Shinde, and PramodNivruttiVasambekar. "Ferrite gas sensors." *Sensors Journal, IEEE* 11.4 (2011): 849-861.

[11] Zampiceni, E., et al. "Composition influence on the properties of sputtered SnWO films." *Sensors and Actuators B: Chemical* 89.3 (2003): 225-231.

[12] Ferro, R., et al. "Gas-sensing properties of sprayed films of (CdO) x (ZnO) 1-x mixed oxide." *Sensors Journal, IEEE* 5.1 (2005): 48-52.

[13] Gaskov, Alexander, and Marina Rumyantseva. "Metal oxide nanocomposites: synthesis and characterization in relation with gas sensing phenomena." *Sensors for Environment, Health and Security*. Springer Netherlands, 2009. 3-30.

[14] Shukla, S., et al. "Nanocrystalline indium oxide-doped tin oxide thin film as low temperature hydrogen sensor." *Sensors and Actuators B: Chemical* 97.2 (2004): 256-265.

[15] Retrieved from http://science1.nasa.gov/science-news/science-at-nasa/2002/06nov_ssme/

[16] Gupta, Ram B., ed. *Hydrogen fuel: production, transport, and storage*. CRC Press, 2008.

[17] Hübert, Thomas, et al. "Hydrogen sensors–a review." *Sensors and Actuators B: Chemical* 157.2 (2011): 329-352.

[18] Gu, Haoshuang, Zhao Wang, and Yongming Hu. "Hydrogen gas sensors based on semiconductor oxide nanostructures." *Sensors* 12.5 (2012): 5517-5550.

[19] Kanan, Sofian M., et al. "Semiconducting metal oxide based sensors for selective gas pollutant detection." *Sensors* 9.10 (2009): 8158-8196.

[20] Auerbach, Scott M., Kathleen A. Carrado, and Prabir K. Dutta. *Handbook of zeolite science and technology*. CRC press, 2003

[21] Cejka, Jiri, et al. *Introduction to Zeolite Molecular Sieves*. Vol. 168. Elsevier, 2007.

[22] Cejka, Jiri, AvelinoCorma, and Stacey Zones, eds. *Zeolites and catalysis: synthesis, reactions and applications*. John Wiley & Sons, 2010.

[23] Kulprathipanja, Santi, ed. *Zeolites in industrial separation and catalysis*. Weinheim, Germany: Wiley-Vch, 2010.

[24] Barquist, Karna Nicole. *Synthesis and environmental adsorption applications of functionalized zeolites and iron oxide/zeolite composites*. Diss. The University of Iowa, 2009.

[25] Xu, Xiaowen, Jing Wang, and Yingcai Long. "Zeolite-based materials for gas sensors." *Sensors* 6.12 (2006): 1751-1764.

[26] Sahner, K., et al. "Zeolites—Versatile materials for gas sensors." *Solid State Ionics* 179.40 (2008): 2416-2423.

[27] Zheng, Yangong, Xiaogan Li, and Prabir K. Dutta. "Exploitation of unique properties of zeolites in the development of gas sensors." *Sensors* 12.4 (2012): 5170-5194.

[28] Mintova, Svetlana, and Thomas Bein. "Nanosized zeolite films for vapor-sensing applications." Microporous and Mesoporous Materials 50.2 (2001): 159-166.

[29] Mintova, Svetlana, Shangyi Mo, and Thomas Bein. "Humidity sensing with ultrathin LTA-type molecular sieve films grown on piezoelectric devices." Chemistry of materials 13.3 (2001): 901-905.

[30] Zhou, Jia, et al. "Zeolite-modified microcantilever gas sensor for indoor air quality control." Sensors and Actuators B: Chemical 94.3 (2003): 337-342.

[31] Huang, Honghu, et al. "A highly sensitive QCM sensor coated with Ag-ZSM-5 film for medical diagnosis." Sensors and Actuators B: Chemical 101.3 (2004): 316-321.

[32] Jung, Man-Kyu, Sung-Sun Hong, and Man-Hoe Kim. "Application of Silicalite-1 film to a surface acoustic wave device sensor." Korean Journal of Chemical Engineering 15.5 (1998): 552-555.

[33] Zhang, Jian, et al. "Zeolite thin film-coated long period fiber grating sensor for measuring trace organic vapors." Sensors and Actuators B: Chemical 135.2 (2009): 420-425.

[34] Wang, Zheng, et al. "Zeolite coated ATR crystals for new applications in FTIR-ATR spectroscopy." Chemical communications 024 (2004): 2888-2889.

[35] Vilaseca, M., et al. "Use of zeolite films to improve the selectivity of reactive gas sensors." Catalysis today 82.1 (2003): 179-185.

[36] Vilaseca, M., et al. "Development and application of micromachinedPd/SnO2 gas sensors with zeolite coatings." *Sensors and Actuators B: Chemical* 133.2 (2008): 435-441.

[37] Binions, Russell, et al. "Discrimination effects in zeolite modified metal oxide semiconductor gas sensors." *Sensors Journal, IEEE* 11.5 (2011): 1145-1151.

[38] Jadsadapattarakul, Damrongsak, et al. "Improved selectivity, response time and recovery time by [010] highly preferred-orientation silicalite-1 layer coated on SnO2 thin film sensor for selective ethylene gas detection." *Sensors and Actuators B: Chemical* 144.1 (2010): 73-80.

[39] Fukui, Kiyoshi, and Sachiko Nishida. "CO gas sensor based on Au–La2 O3added SnO2 ceramics with siliceous zeolite coat." *Sensors and Actuators B: Chemical* 45.2 (1997): 101-106.

[40] Hugon, Olivier, et al. "Gas separation with a zeolite filter, application to the selectivity enhancement of chemical sensors." Sensors and Actuators B: Chemical 67.3 (2000): 235-243.

[41] Mann, D. P., et al. "Metal oxide semiconductor gas sensors utilizing a Cr-zeolite catalytic layer for improved selectivity." *Measurement Science and Technology* 16.5 (2005): 1193.

[42] Mann, Dominic P., et al. "Transition metal exchanged zeolite layers for selectivity enhancement of metal-oxide semiconductor gas sensors." Sensors Journal, IEEE 7.4 (2007): 551-556.

[43] Fong, Yeong Yin, et al. "Zeolite membrane based selective gas sensors for monitoring and control of gas emissions." Sensor Letters 5.3-4 (2007): 3-4.

[44] Mann, D. P., et al. "Metal oxide semiconductor gas sensors utilising modified zeolite catalysts to improve selectivity." Sensors, 2004. Proceedings of IEEE. IEEE, 2004.

[45] Trimboli, Joseph, and Prabir K. Dutta. "Oxidation chemistry and electrical activity of Pt on titania: development of a novel zeolite-filter hydrocarbon sensor." Sensors and Actuators B: Chemical 102.1 (2004): 132-141.

[46] Meier, Brit, et al. "Novel oxygen sensor material based on a ruthenium bipyridyl complex encapsulated in zeolite Y: dramatic differences in the efficiency of luminescence quenching by oxygen on going from surface-adsorbed to zeolite-encapsulated fluorophores." Sensors and Actuators B: Chemical 29.1 (1995): 240-245.

[47] Meier, Brit, et al. "Novel oxygen sensor material based on a ruthenium bipyridyl complex encapsulated in zeolite Y: dramatic differences in the efficiency of luminescence quenching by oxygen on going from surface-adsorbed to zeolite-encapsulated fluorophores." Sensors and Actuators B: Chemical 29.1 (1995): 240-245.

[48] Payra, Pramatha, and Prabir K. Dutta. "Development of a dissolved oxygen sensor using tris (bipyridyl) ruthenium (II) complexes entrapped in highly siliceous zeolites." Microporous and mesoporous materials 64.1 (2003): 109-118.

[49] Zou, Jing, et al. "A guest/host material of LiCl/H-STI (stilbite) zeolite assembly: preparation, characterization and humidity-sensitive properties." Journal of Materials Chemistry 14.15 (2004): 2405-2411.

[50] Li, Nan, et al. "Host–guest composite materials of LiCl/NaY with wide range of humidity sensitivity." Materials Letters 58.10 (2004): 1535-1539.

[51] Sohrabnezhad, Shabnam, AfshinPourahmad, and Mir AbdollahSadjadi. "New methylene blue incorporated in mordenite zeolite as humidity sensor material." Materials Letters 61.11 (2007): 2311-2314.

[52] Zanjanchi, M. A., and ShSohrabnezhad. "Evaluation of methylene blue incorporated in zeolite for construction of an optical humidity sensor." Sensors and Actuators B: Chemical 105.2 (2005): 502-507.

[53] Pellejero, Ismael, et al. "An optochemical humidity sensor based on immobilized nile red in Y zeolite." Industrial & engineering chemistry research 46.8 (2007): 2335-2341.

[54] Larsen, Sarah C. "Nanocrystalline zeolites and zeolite structures: synthesis, characterization, and applications." The Journal of Physical Chemistry C 111.50 (2007): 18464-18474.

[55] Song, Weiguo, et al. "Development of improved materials for environmental applications: NanocrystallineNaY zeolites." Environmental science & technology 39.5 (2005): 1214-1220.

[56] Li, Qinghua, Derek Creaser, and Johan Sterte. "An investigation of the nucleation/crystallization kinetics of nanosized colloidal faujasite zeolites." Chemistry of materials 14.3 (2002): 1319-1324.

[57] Watts, John F., and John Wolstenholme. "An introduction to surface analysis by XPS and AES." *,pp. 224. ISBN 0-470-84713-1. Wiley-VCH, May 2003.* 1 (2003).

[58] Rodney Herring. “Introduction to Scaning electron microscopy”

[59] Vij, D. R. “Handbook of Applied Solid State Spectroscopy”. Springer, 2006

[60] Treacy, Michael MJ, John B. Higgins, and Roland von Ballmoos. *Collection of simulated XRD powder patterns for zeolites*. Vol. 552. New York: Elsevier, 1996.

[61] Isernia, Luis Fioravanti. "FTIR study of the relation, between extra-framework aluminum species and the adsorbed molecular water, and its effect on the acidity in ZSM-5 steamed zeolite." *Materials Research*, 2013.

[62] Datka, J., and E. Tużnik. "Hydroxyl groups and acid sites in Na- ZSM-5 zeolites studied by ir spectroscopy." *Zeolites* 5.4 (1985): 230-232.

[63] Jansen, J. C., F. J. Van der Gaag, and H. Van Bekkum. "Identification of ZSM-type and other 5-ring containing zeolites by ir spectroscopy." *Zeolites* 4.4 (1984): 369-372.

[64] Wagner, C. D., et al. "Handbook of XPS Perkin-Elmer Corporation." *Eden Prairie* (1992).

VITAE

Personal Information

Name: Anas Awad Hasan Ahmed

Date of Birth: December 20, 1983, Taiz, Yemen

Contact: Phys. Dept., Taiz University, Yemen

Email Address: anasawad21yahoo.com

Education

May, 2014: Master in physics, KFUPM, Saudi Arabia.

2004-2008: B.S. Physics, Taiz University, Yemen.

2001-2003: Diploma in Pharmacy, National University, Yemen.

Training and Experience

Nov 2008 –Jul 2010: Instructor in Physics Dept., Faculty of Science, Taiz University, Yemen.

July- 2007: Training course in experimental physics, Menoufia University, Egypt.